Economic Geology, v. 103, pp. 1341–1363

Lithogeochemical and Stratigraphic Controls on Gold Mineralization within the Metavolcanic Rocks of the Hoyle Pond Mine, Timmins, Ontario

Etienne Dinel,† Anthony D. Fowler,

Department of Earth Sciences, University of Ottawa, 140 Louis Pasteur St., Ottawa, Canada K1N 6N5, and Ottawa Carleton Geoscience Centre

John Ayer,

Ontario Geological Survey, Precambrian Science Division, 933 Ramsey Lake Rd, Sudbury, Ontario, Canada P3E 6B5

Alastair Still, Ken Tylee, and Erik Barr

Porcupine Joint Venture, Hoyle Pond Mine, 1 Gold Mine Road, P.O. Box 70, Timmins, Ontario, Canada P0N 1G0

Abstract

The Hoyle Pond gold deposit is hosted in complexly deformed mafic-ultramafic volcanic rocks of the Hersey Lake and Central Formations (Tisdale assemblage) in the Porcupine gold camp, located approximately 15 km northeast of Timmins in the Abitibi greenstone belt. The deposit is hosted within a homoclinal sequence of south-facing stacked volcanic flows of high Mg tholeiitic basalt, basaltic komatiite and komatiite flows, and interbedded high Mg tholeiitic basalt and Fe-rich tholeiitic basalts. The bulk of the gold mineralization was emplaced at lithologic contacts along late shear zones associated with isoclinal folding and thrusting. The mineralization is characterized by micron- to centimeter-sized flakes of free gold or veinlets in quartz-carbonate (dolomite and ferroan dolomite) shear and extension vein arrays. At the mine scale a broad carbonate alteration is evident. Two alteration zones surrounding the veins were mapped at the meter scale: an inner sericite alteration zone composed of sericite (muscovite), fuchsite (Cr muscovite), quartz, arsenopyrite, pyrite, ferroan-dolomite, dolomite, and graphite plus tourmaline, and an outer zone of albite alteration consisting of albite, quartz, ferroan dolomite, and dolomite.

Geochemical analyses of 355 samples show that the REE, Zr, Al_2O_3, TiO_2, and Y were largely immobile during alteration and mineralization. CO_2, K_2O, Na_2O, Cr_2O_3, Rb, As, B, SiO_2, and CaO, and locally Fe_2O_3, FeO, and MgO, were mobile during alteration and mineralization. The chromium enrichment is not primary and is interpreted to have been caused by remobilization from ultramafic rocks during mineralization. In addition, an intense graphite alteration, originally derived from organic matter, probably from sedimentary rocks, and now associated with mineralization, is present in zones that were porous and permeable at the time of mineralization. In common with other mesozonal orogenic gold deposits, gold was likely transported as a thio complex. The Cr enrichment in the wall rock indicates that Cr was mobile, most likely as Cr^{6+}. Because species such as Cr^{6+} are transported under oxidizing conditions and carbon and Au-HS species are transported under reduced conditions, we suggest that more than one fluid was involved in the mineralization and/or alteration. Mixing between reducing and oxidizing fluids is thought to have reduced Cr^{6+} to Cr^{3+}, oxidized the organic matter to form graphite, oxidized sulfur to form sulfides, and precipitated Au. This is consistent with the observed paragenesis. Reducing fluids rich in boron, arsenic, carbon, and Au may have been generated from sedimentary rocks (Porcupine assemblage?) at depth and expelled during orogenesis into syndeformation structures within overlying volcanic rocks where they mixed with oxidizing fluids containing Cr, K_2O, SiO_2, Na_2O, and CaO.

Introduction

The Hoyle Pond mine is located 15 km east of downtown Timmins and 3 km north of the Pamour mine in the Porcupine gold camp of the Archean Abitibi subprovince of the Superior province, northern Ontario (Fig. 1). The discovery hole was drilled by Texas Gulf in 1980, and the mine has been in constant production since 1985. The mineralization is associated with fault-fill and extensional quartz-carbonate veins along second-order shear zones and faults spatially related to the Porcupine-Destor deformation zone. It is hosted by ultramafic and mafic metavolcanic rocks of the Tisdale assemblage (2710–2704 Ma: Ayer et al., 2005), which is subdivided in the mine into three volcanic packages, namely, the north, the central and the south volcanic packages (NVP, CVP and SVP, respectively; Fig. 2). Prior to 1994, most of the ore was mined from the Hoyle Pond zone (13–14 and 16 veins) in mafic rocks of the north volcanic package. Subsequently, in 1994, with the discovery of the 1060 zone, the A-vein zone, and the 7-veins zone, the main focus of production switched to the south volcanic package. Currently, production comes predominantly from the A vein and the 1060 fault zone, which extend vertically to depths of greater than 1,000 m.

This paper describes the geology (stratigraphy, structural geology, alteration, and mineralization) of the Hoyle Pond deposit and identifies critical host-rock chemical and physical factors that contributed to the localization of gold mineralization. The geology of the Hoyle Pond deposit is compared to other deposits in the Timmins Porcupine camp, and these results are integrated into a model describing the structural and hydrothermal evolution of the Hoyle Pond mine.

† Corresponding author: e-mail, edinel@nrcan.gc.ca

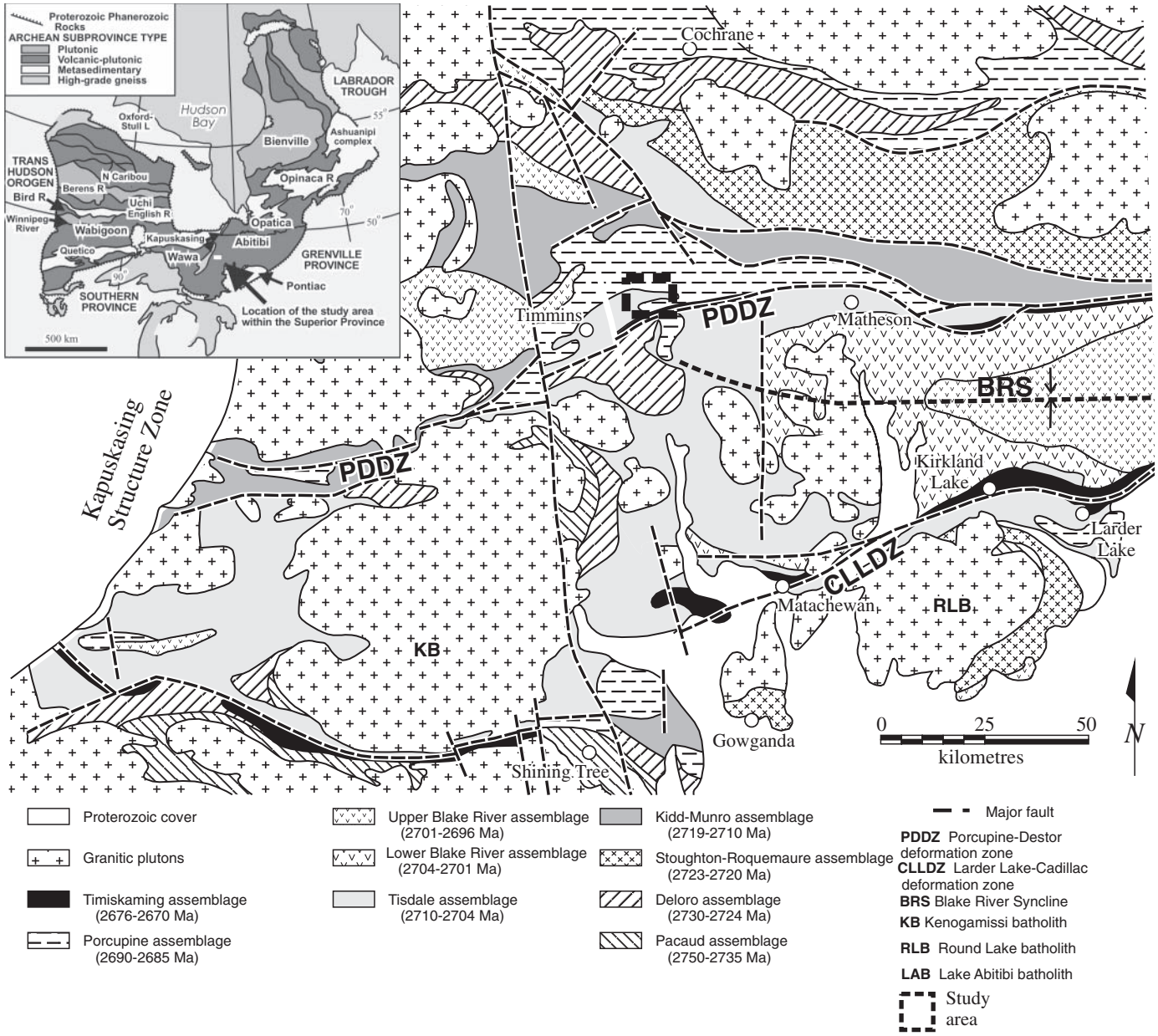

FIG. 1. Geologic map of the Abitibi greenstone belt, illustrating the nine volcano-sedimentary rock assemblages as defined by Ayer et al. (2005). The Hoyle Pond gold mine is located in the Tisdale assemblage of the Abitibi South volcanic zone and the mine area is outlined by dashed line box.

Methodology

Mapping

Four levels in the mine were mapped for the project. The two main levels, the 440-m and the 720-m levels, were investigated to define the stratigraphy of the mine (Fig. 2) and to verify the continuity of the stratigraphy vertically. Two other levels were investigated: to understand the origin of the 1060 fault zone (the 880-m level 1060 crosscut) and to determine the control on emplacement of the mineralization in the north volcanic package (the 400-m level; Hoyle Pond mine 3 level).

Sampling, sample preparation, and laboratory analysis

Three hundred and fifty-five samples were analyzed for whole-rock geochemistry (major oxides and trace elements) from the 3 level (400-m level, 16 vein zone), the 440-m level (950 zone and 16 vein zone), the 720-m level (1060 zone), the 880-m level (1060 zone), and drill core. Analytical data and locations are given in Dinel (2007).

Major and trace elements were analyzed by XRF and ICP-MS, respectively, at the University of Ottawa, Ottawa, Ontario, and the Ontario Geoscience Laboratories, Sudbury, Ontario. Ferrous iron was determined by the modified Wilson (1960) technique (Whipple, 1974). The error in the major

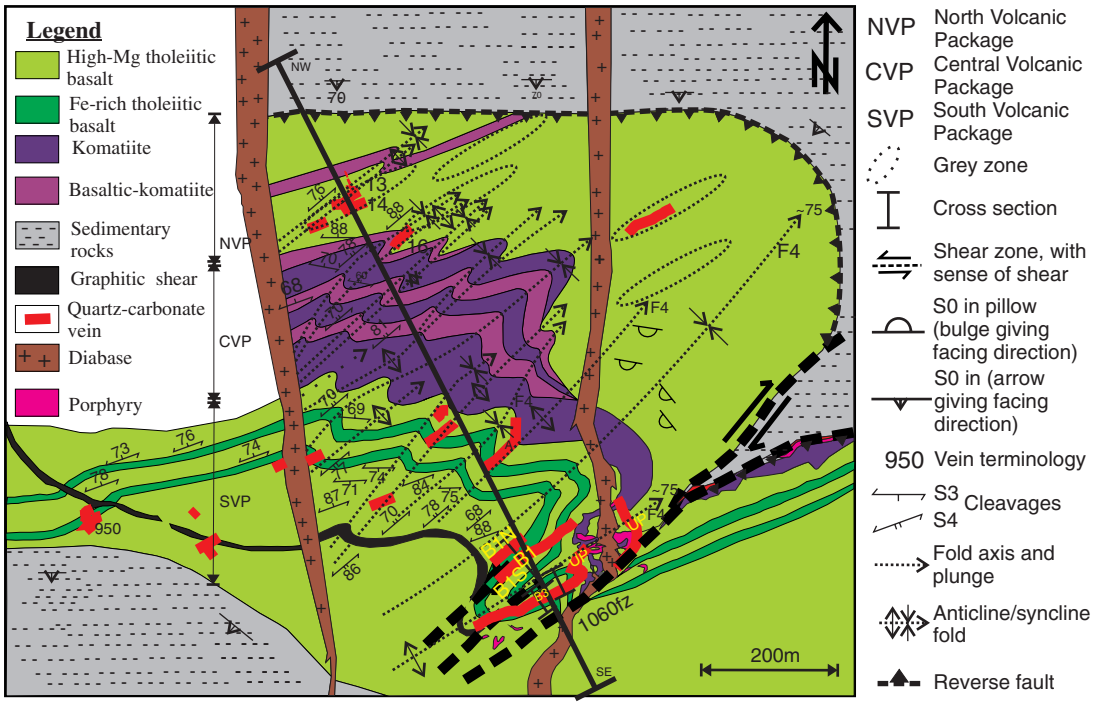

FIG. 2. Simplified geologic map of the Hoyle Pond mine, compiled from the 440- and 720-m level maps. Certain veins are labeled using the mine convention (e.g., "A" vein). Traverses across veins are indicated. Note that in the western portion of the south volcanic package, the graphitic unit cuts the stratigraphy.

oxides is less than 0.5 percent of the reported value and for trace elements, less than 10 percent. The error was calculated with a confidence interval of 95 percent, using the method of Kretz (1985) on lab standards and on three blind samples analyzed five times in repetition. Two blank samples were analyzed to identify contaminants.

Analyses of alteration minerals were done using the electron microprobe at Carleton University, Ottawa, Ontario. Carbon isotopes were measured by Vario EL III (Elementar, Germany) and DeltaPlus IRMS (ThermoFinnigan, Germany) at the University of Ottawa to determine the relative and absolute concentration of ^{13}C. Organic matter in graphite was extracted from the powdered rock samples by NaOH hydrolization and was analyzed using a spectrophotometer which measures the absorption of light in the ultraviolet wavelength range.

Regional Geologic Setting

The Archean bedrock geology of the Timmins gold camp consists of four distinct supracrustal units identified as the Deloro, Tisdale, Porcupine, and Timiskaming assemblages. These assemblages are cut by different suites of intrusions (Fig. 3A), which are defined by their geochronologic age (U-Pb TIMS), tectonic affinity, and geochemical signatures. The Tisdale and Porcupine assemblages are the only assemblages present at Hoyle Pond and are described below.

Tisdale assemblage

The Tisdale assemblage is mainly composed of mafic tholeiitic volcanic rocks, intercalated with ultramafic and felsic volcanic rocks, and of felsic calc-alkaline volcanic rocks (Fig. 3A) ranging in age from 2710 to 2704 Ma (Ayer et al., 2005). South of the Porcupine-Destor deformation zone, the Tisdale assemblage unconformably overlies the Deloro assemblage. The maximum apparent thickness of the Tisdale assemblage is 3,440 m as measured in the northeastern part of Tisdale Township between the axis of the North Tisdale anticline and its upper contact with the Krist Formation (Brisbin, 1997). Previous authors interpret the base of the Tisdale assemblage to be within the Porcupine Destor deformation zone (Pyke, 1982). However, field mapping by Dinel and others (Vaillancourt et al., 2001; Bateman et al., 2005) show that the location of the Porcupine-Destor deformation zone is neither restricted to the base of the Tisdale assemblage nor is it a discrete fault surface. Instead it is a large (100–500 m) corridor of deformation overprinting the unconformity. The Tisdale assemblage (formerly a group) is subdivided into five formations (Dunbar, 1948, Jones, 1948; Ferguson et al., 1968), two of which, the Central and Vipond Formations, host the majority of the economic deposits. The formations are briefly described below in ascending stratigraphic order.

Hersey Lake Formation: The Hersey Lake Formation consists mainly of high Mg tholeiitic basaltic pillowed flows, basaltic komatiitic, and komatiitic flows. It has an apparent thickness of ~600 m (Brisbin, 1997).

The ultramafic flows are classified as basaltic komatiite and komatiite based on the geochemical criteria of Arndt (1975), with MgO contents of 10 to 18 and >18 wt percent. They have flat REE patterns with chondrite ratios <7. In the field, the ultramafic flows of the Hersey Lake Formation can be distinguished from the mafic flows by their color index and characteristic polygonal jointing. Komatiites are dark gray, on fresh

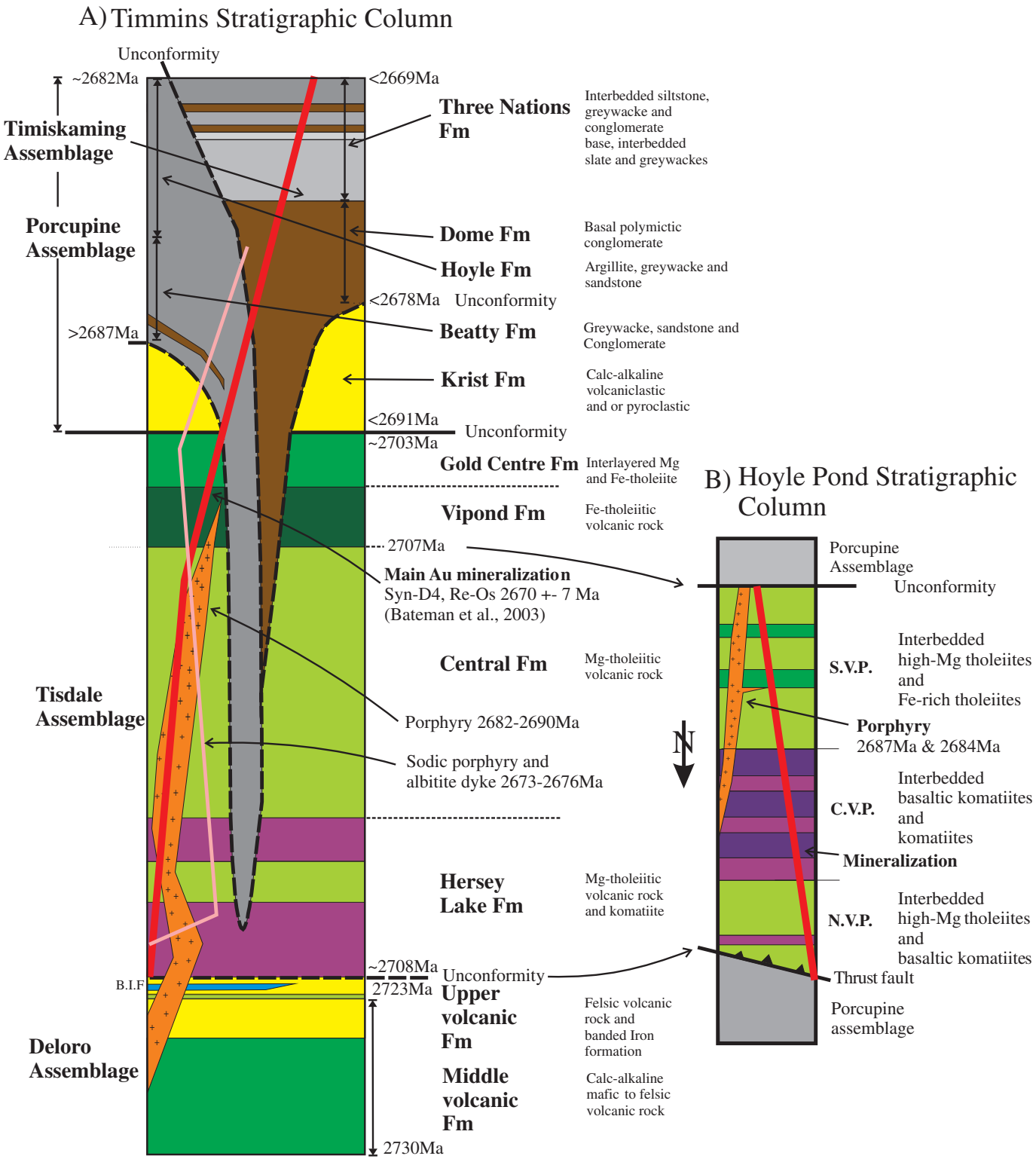

FIG. 3. A. Stratigraphic column of the Timmins area (modified from E. Barr, Porcupine Joint Venture internal report, 2005). B. Stratigraphic column of the Hoyle Pond mine. C.V.P. = central volcanic package, N.V.P. = north volcanic package, S.V.P. = south volcanic package. The mine rocks are within the Hersey Lake and Central Formations of the Tisdale assemblage.

surfaces, and have an orange-brown color on weathered surfaces. In addition, some komatiite flows have spinifex textures and are altered to talc and carbonate and cut by serpentine-filled fractures. The tholeiitic mafic volcanic rocks within the Hersey Lake Formation occur as massive and pillowed flow and differ from similar flows in the overlying Central Formation by their association with ultramafic flows.

Central Formation: Pyke (1982) described the composition of the mafic volcanic flows of the Central Formation as a continuum from magnesium tholeiitic basalts through iron tholeiitic basalts. The Central Formation is approximately 450 m thick (Brisbin, 1997) and is mainly composed of mafic, locally variolitic, massive, and pillowed flows with pillow top breccias. Pillows have 1- to 5-cm-thick selvages and an average size of 100 × 50 cm in plan view. The rocks of the Central Formation are in general high Mg basalts intercalated with beds of black argillite or siltstones with cherty clasts.

Vipond Formation: The Vipond Formation is characterized by very distinctive high Fe tholeiitic variolitic pillowed mafic and intermediate volcanic flows (Dinel et al., 2008) and by variolitic hyaloclastic mafic flows intercalated with massive mafic flows and carbonaceous argillite.

Gold Centre Formation: The Gold Centre Formation is the uppermost formation of the Tisdale assemblage. It is dominated by green, fine- to medium-grained, massive, leucoxene-bearing mafic flows (likely tholeiitic basalts) and calc-alkaline mafic to felsic volcanic rocks (Brisbin, 1997).

Porcupine assemblage

The Porcupine assemblage ranges in age from 2690 to 2685 Ma and unconformably overlies the Tisdale assemblage in the Timmins area (Ayer et al., 2005). It is composed of siltstone, mudstone, and sandstones with local polymictic conglomerate, in conformable contact with calc-alkaline felsic volcanic rocks of the Krist Formation at the base of the assemblage (Fig. 3A). The turbidites have Bouma sequence subdivisions indicating distal deposition from turbidity currents in a shelflike environment (Born, 1995). It is a very extensive assemblage, occurring north of the Porcupine-Destor deformation zone from Bristol Township, 20 km west of Timmins, to Matheson, over a distance of approximately 80 km.

Major regional structures

The Porcupine-Timmins gold camp is deformed by at least six deformation events (D_1–D_6: Bleeker, 1999; Bateman et al., 2005). The first two events, D_1 and D_2, are not observed at Hoyle Pond and will not be discussed further. D_3 is represented by east-west–trending isoclinal folds with a steeply dipping axial planar S_3 foliation parallel to lithologic contacts. D_3 is either syn- or postdeposition of the Timiskaming assemblage (Bateman et al., 2005). D_4 produced a steeply dipping foliation, S_4, oriented ~060° to 070°, ~15° counterclockwise to S_3. S_4 is axial planar to isoclinal F_4 folds, which correspond to the northern margin of the 1060 fault zone in Hoyle Pond. The intersection lineation of S_3 (E-W) with S_4 (ENE-WSW) appears to be subparallel to the plunge of ore zones at the Hollinger-McIntyre deposit (Melnik-Proud, 1992) and Hoyle Pond mine. The D_5 event is represented by a moderately dipping crenulation cleavage, S_5, with two general strikes of 045° and 335°. S_5 is axial planar to asymmetric Z and S folds. D_6 structures are observed on vertical surfaces as a subhorizontal crenulation, S_6 cleavage, axial planar to millimeter- to meter-scale subhorizontal folds (Dinel, 2001).

The major shear zone in the Timmins area, the Porcupine-Destor deformation zone is a high-strain corridor with intense foliations, characterized by tight to isoclinal F_4 folds. The Hollinger-McIntyre and Dome mines occur on structures that are subparallel splays of the Porcupine-Destor deformation zone.

Mine Geology and Volcanic Geochemistry

The volcanic belt is bounded on all sides by metasedimentary rocks of the Porcupine assemblage (Rye, 1987; Fig. 2). The volcanic rocks at the mine are thrust bounded to the north by south-facing graywackes and siltstones of the Porcupine assemblage and to the south by discordance (either a fault or unconformity) at their contact with south-facing siltstones and graywacke, also of the Porcupine assemblage (2690–2685 Ma: Ayer et al., 2005). The volcanic rocks are intruded by quartz-feldspar porphyries and quartz porphyries (Fig. 2).

The volcano-sedimentary rocks in the Hoyle Pond area were subjected to greenschist facies regional metamorphism (e.g., Thompson, 2005). Throughout the area, undeformed and deformed volcanic rocks are composed of an albite-chlorite mineral assemblage, the pores spaces (clast interstices and vesicles) of which have been filled with calcite, minor quartz, and chlorite.

The volcanic geochemistry of units exposed in the mine was determined by meter-scale sampling. The elements Al, Ti, HREE, Zr, and Y, and to a lesser extent LREE, were interpreted to be "immobile" (see Fig. 4A), consistent with previous work by Kerrich et al. (1999) and Wyman (2003). Chondrite-normalized plots (Sun and McDonough, 1989) and various trace element ratio plots were used to help discriminate rock types and to compare the stratigraphy of the Hoyle Pond with formations within the Tisdale assemblage.

North volcanic package

The north volcanic package consists of interbedded mafic and ultramafic volcanic rocks (Fig. 2). The mafic rocks are dominated by pillowed flows, pillow breccias, and locally massive coherent flows (Fig. 5A). The pillows vary in size from 50 cm to 1.5 m. They are generally undeformed and south facing outside of shear zones, consistent with the facing direction of the Porcupine metasedimentary rocks bounding the mine stratigraphy to the north and south (cf. Rye, 1987). They are characterized by a pale apple-green color and a very fine grained groundmass. On level 3 of the mine, variolitic pillow flows and pillow breccias were observed. Variolitic pillows exhibit leucocratic millimeter-scale (2–5 mm) globular bodies which are aligned and form bands along pillow margins. In thin section the varioles appear as very fine, 2- to 5-mm spherulites that have diffuse edges that blend with the groundmass. They are albitized and contain patches of titanite. Pervasively albitized rocks have fanlike albite in microlithons with spherulitic extinction. Fragments in the pillow breccia are amoeboidal and vary in size from 5 to 25 cm with millimeter-size varioles that are concentrated in sinuous bands and are truncated by the pillow selvages (Fig. 5B). The

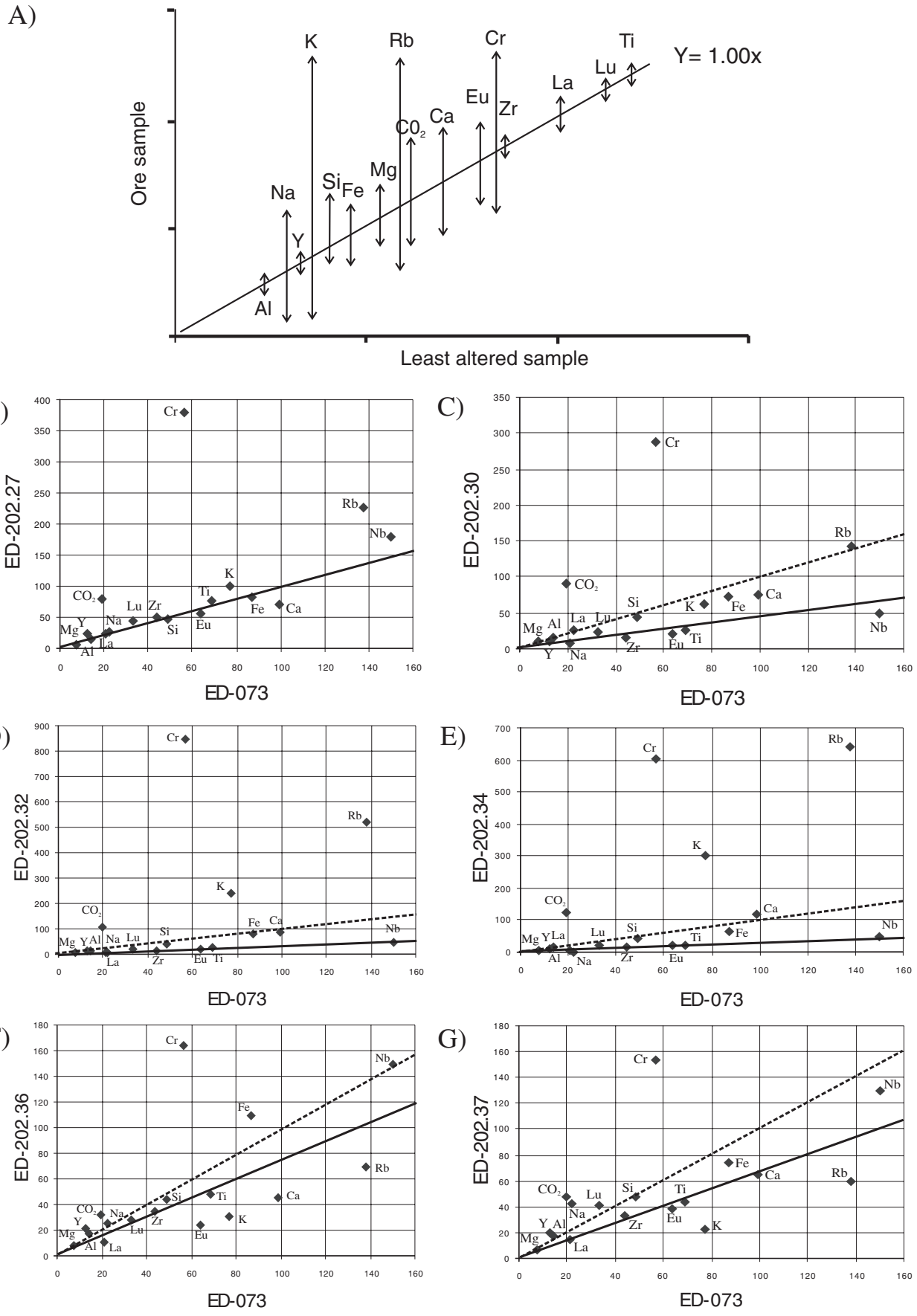
A)
Ore sample
Least altered sample
Y= 1.00x
K
Rb
Cr
Ti
Lu
La
Eu
Zr
Ca
$C0_2$
Mg
Si
Fe
Na
Y
Al
B)
ED-202.27
ED-073
C)
ED-202.30
ED-073
D)
ED-202.32
ED-073
E)
ED-202.34
ED-073
F)
ED-202.36
ED-073
G)
ED-202.37
ED-073

mafic rocks are composed of chlorite, albite, carbonate, hydrothermal quartz, and sericite, and some opaque minerals (chiefly graphite, minor iron oxides, pyrite, and traces of chalcopyrite). Locally, sericite is concentrated along cleavage domains.

The ultramafic rocks are dark gray to black aphanitic rocks with coarser grained dolomite porphyroblasts and a soapy-soft cleavage. They locally contain minor chlorite, some disseminated quartz crystals, and iron oxides.

On the Jensen cation diagram, high Mg tholeiitic basalts are displaced toward aluminum and into the calc-alkaline field (Fig. 6A) due to the mobility of MgO and FeO (i.e., a loss of FeO and MgO relative to Al_2O_3). The mafic rocks plot mostly in the high Mg tholeiitic field of the Jensen cation plot with some samples appearing in the calc-alkaline basaltic field (Fig. 6A). Although Fe and Mg were mobile, the geochemical signature of the high Mg tholeiite can be identified by their generally flat, slightly concave REE patterns (Fig. 6B). The HREE (Gd, Dy, Er, Yb, Lu) are in general slightly more enriched than the LREE (La, Ce, Nd, Sm). The LREE have flat to shallow negative slope (La-Sm) varying from 3 to 14 times chondrite; the HREE have a gently positive slope varying from 12 to 20 times chondrite. The La/Lu and Ce/Yb chondrite-normalized ratios range from 0.2 to 0.8 and 0.3 to 0.8, respectively. Although most samples have negative Eu anomalies, others have positive Eu anomalies. The positive Eu anomalies may represent the deposition of Eu-bearing carbonate minerals from relatively Eu rich fluids (Michard and Albarède, 1986).

In contrast, the REE concentrations of basaltic komatiites (Fig. 6B) are less than 10 times chondrite and show convex REE patterns with enriched HREE compared to LREE. The normalized LREE abundances vary from 5.5 to 7.5 times chondrite, and the normalized HREE abundances vary from 8.0 to 9.5 times chondrite. Eu anomalies vary from slightly positive to slightly negative. The La/Lu and Ce/Yb chondrite-normalized ratios range from 0.4 to 0.8 and 0.5 to 0.8, respectively.

Central volcanic package

The Central volcanic package (CVP; Fig. 2) consists of a sequence of interbedded komatiite (typically >18 wt % MgO) and basaltic komatiites (12–18 wt % MgO; Fig. 7A) approximately 200 m in apparent thickness. The contacts between the basaltic komatiites and komatiites are gradational and are commonly overprinted by strong carbonate alteration (dolomite to ferroan dolomite) and deformation, which resulted in the generation of an intense fabric and associated quartz-carbonate stringer zones.

The basaltic komatiites are carbonatized fine- to medium-grained dark green to black chlorite schists with minor talc. The mineral assemblage is dominated by chlorite, talc, dolomite, hydrothermal quartz, iron-titanium oxides, coarse-grained (1–2 mm) carbonate porphyroblasts and locally Cr micas, actinolite, and trace pyrite.

The komatiites are talc-chlorite schist or talc schist. Their color varies from dark gray-black to cream gray-beige due to carbonatization. The mineral assemblage is dominantly talc, chlorite, dolomite, hydrothermal quartz, iron-titanium oxides, and locally serpentine. In some thin sections, the Fe-Ti oxide crystals form ringlike structures typical of relict olivine and are interpreted to represent the remnants of olivine cumulate zones (Fig. 5C).

With one exception, all samples of the central volcanic package have REE concentrations less than 10 times chondrite (Fig. 7B). The HREE patterns have less curvature than the LREE and a slight decrease in concentration from Dy to Lu. Some samples have slight positive Eu anomalies, whereas the majority have small negative Eu anomalies. There is a continuum in REE concentrations from komatiites to basaltic komatiites. The komatiites have normalized LREE abundances from 1.5 to 3.5 times chondrite and normalized HREE abundances from 3.0 to 5.5 times chondrite. The La/Lu and Ce/Yb chondrite-normalized ratios range from 0.3 to 1.0 and 0.3 to 1.2, respectively. The basaltic komatiites have normalized LREE of 4.0 to 8.0 times chondrite and normalized HREE abundances from 6.5 to 10 times chondrite. The La/Lu and Ce/Yb chondrite-normalized ratios range from 0.4 to 0.8 and 0.5 to 0.9, respectively.

South volcanic package

The south volcanic package rocks (Fig. 2) are strongly carbonatized basalts and possess a more pervasive foliation than rocks of the north and central volcanic packages. They occur as, pale to dark green ~10- to 40-m-thick massive to pillowed flows with local flow top breccias, which were deformed to coarse-grained chloritic schist. Their mineralogy consists of

FIG. 4. A. Schematic isocon diagram (Grant, 1986) of an altered sample on the south volcanic package 720-m level 1060 fault zone, demonstrating the mobility of some trace elements (ppm) and major oxides (wt %). B. Scaled isocon plot of sample ED-202.27 compared to the least altered sample ED-073. Sample ED-202.27 is located 4 m away from the B3 vein, a stockwork zone. C. Scaled isocon plot of sample ED-202.30 compared to the least altered sample ED-073. Sample ED-202.30 is located 1 m away from the B3 vein. D. Scaled isocon plot of sample ED-202.32 compared to the least altered sample ED-073. E. Scaled isocon plot of sample ED-202.34 compared to the least altered sample ED-073. Samples ED-202.32 and ED-202.34 are located in the stockwork zone of the B3 vein. Note the strong increase in Cr, K_2O, and Rb concentration. F. Scaled isocon plot of sample ED-202.36 compared to the least altered sample ED-073. G. Scaled isocon plot of sample ED-202.37 compared to the least altered sample ED-073. Samples ED-202.36 and ED-202.37 are located 13 and 14 m, respectively, away from the B3 vein. Note the concentration decrease in Cr, K_2O, and Rb and concentration increase in Na_2O. The solid line in the diagrams connects the immobile elements. If the trace elements define a straight line of slope equal to one, they have not been perturbed. In highly altered samples, the trace elements would scatter. However, if they define a straight line of slope less than one, the trace element concentrations are diluted. The dashed line is a reference line with a slope of 1. Note that the units are in wt percent for major oxides and ppm for trace elements multiplied by a factor. Al = Al_2O_3 wt %, Mg = MgO wt % × 1, Ti = TiO_2 wt % × 100, Zr = ppm × 1, Na = Na_2O wt % × 10, K = K_2O wt % × 100, Ca = CaO wt % × 10, Rb = ppm × 10, Eu = ppm × 100, Cr = ppm × 1, Y = ppm × 1, La = ppm × 10, Lu = ppm × 100, Lu = ppm × 100, Fe = FeO wt % × 10, Nb = ppm × 100, Si = SiO_2 wt % × 1.

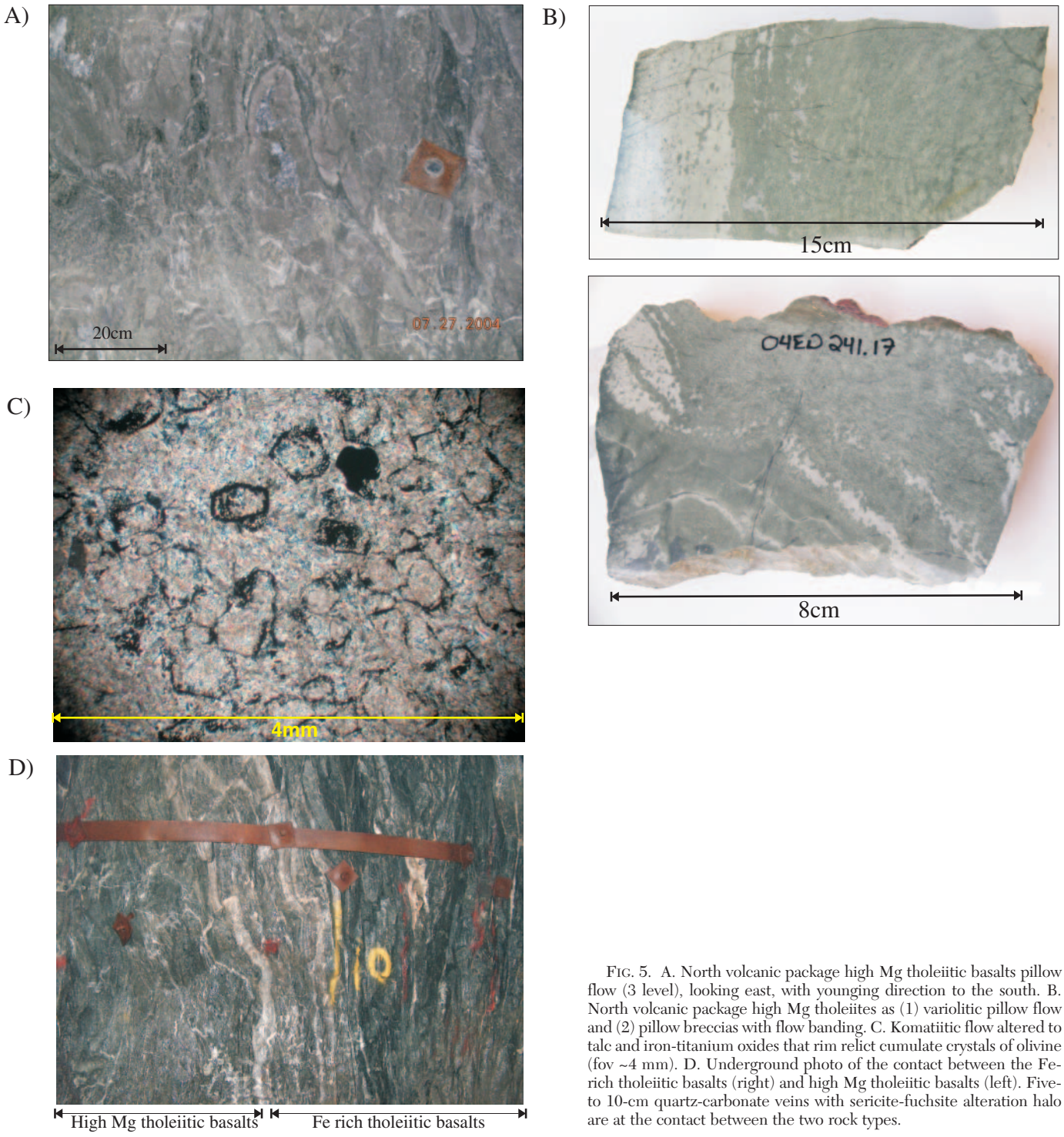

FIG. 5. A. North volcanic package high Mg tholeiitic basalts pillow flow (3 level), looking east, with younging direction to the south. B. North volcanic package high Mg tholeiites as (1) variolitic pillow flow and (2) pillow breccias with flow banding. C. Komatiitic flow altered to talc and iron-titanium oxides that rim relict cumulate crystals of olivine (fov ~4 mm). D. Underground photo of the contact between the Fe-rich tholeiitic basalts (right) and high Mg tholeiitic basalts (left). Five- to 10-cm quartz-carbonate veins with sericite-fuchsite alteration halo are at the contact between the two rock types.

chlorite, quartz, titanite, sericite, carbonate (calcite, dolomite, and ferroan dolomite), K feldspar, pyrite, iron-titanium oxides, and locally, graphite.

The composition of the carbonate mineral differs in the Fe-rich tholeiitic basalts, where it is more enriched in Fe (ferroan dolomite). In addition, the high Mg and Mg tholeiitic basalts show slight modal increase in pyrite and chalcopyrite. Contacts between the three units are sharp and marked by quartz veining, Cr mica, and sericite alteration (Fig. 5D). They are pale to dark green and occur as medium- to coarse-grained chlorite schist. The pillows and breccia clasts in the 1060 fault zone are stretched vertically, parallel to the S_3-S_4 intersection lineation.

The three compositional groups are observed in the Jensen cation plot (Fig. 7C), chondrite-normalized REE plot (Fig. 7D), and plot of Zr/Al_2O_3 vs. TiO_2/Al_2O_3 (Fig. 7E). The Fe-rich

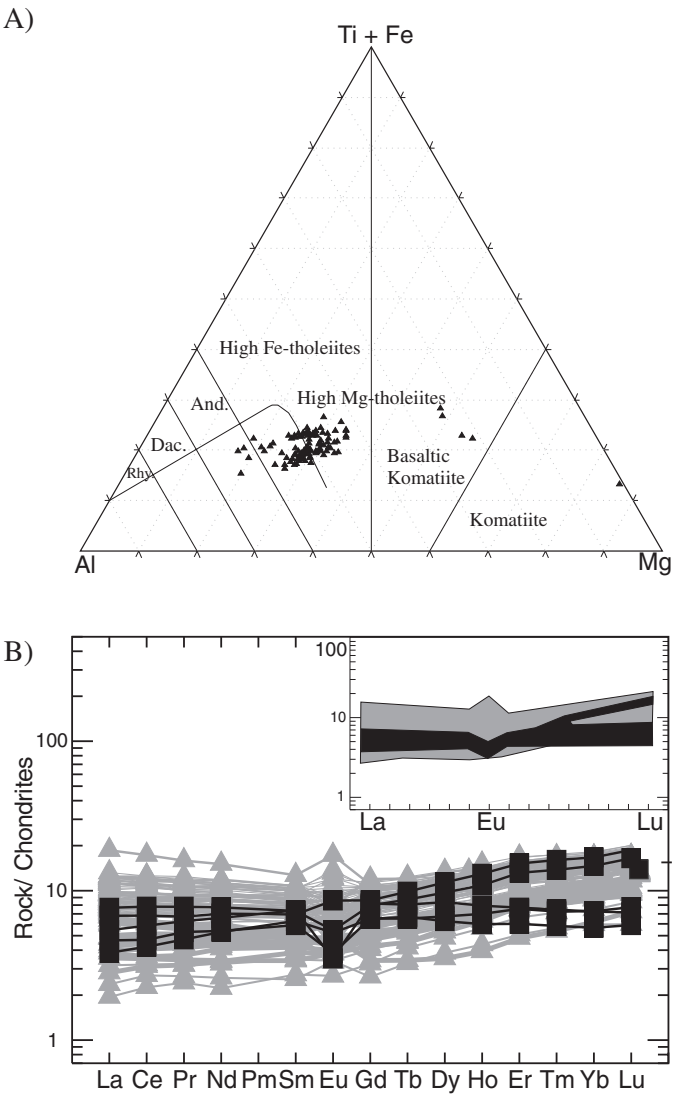

FIG. 6. A. Jensen cation plot (Jensen, 1976) of the north volcanic package volcanic rocks which plot in the field of high Mg tholeiitic basalts and basaltic komatiites. B. Chondrite-normalized REE pattern of the north volcanic package high Mg tholeiitic basalts and basaltic komatiites. The inset shows the approximate range of the normalized REE abundance of the high Mg tholeiitic basalts (gray) and basaltic komatiites (black).

tholeiitic basalts are characterized by their relatively high REE concentrations and concave LREE to HREE pattern, with HREE slightly more enriched than LREE. The normalized LREE abundances vary from 15 to 30 times chondrite, and the normalized HREE abundances vary from 20 to 30 times chondrite (Fig. 7D). The La/Lu and Ce/Yb ratios range from 0.4 to 0.8 and 0.5 to 0 0.9, respectively. The REE concentration of Mg tholeiitic basalts have slopes similar to those of the Fe-rich tholeiitic basalts and high Mg tholeiitic basalts but have intermediate REE concentrations. The LREE concentrations vary from 6.0 to 11 times chondrite and the HREE concentrations vary from 8.0 to 15 times chondrite (Fig. 7D). The La/Lu and Ce/Yb ratios range from 0.4 to 0.9 and 0.5 to 0.9, respectively. The Mg tholeiites plot in the same location as other Mg basalts observed in the north volcanic package in the Jensen diagram. The REE patterns of the high Mg tholeiitic basalts are similar to those of the other two basalt types, but they are characterized by lower REE abundances with normalized LREE abundances that vary from 2.2 to 4.7 times chondrite and normalized HREE abundance that vary from 7.0 to 11 times chondrite (Fig. 7D). The La/Lu and Ce/Yb ratios range from 0.3 to 0.7 and 0.3 to 0.7, respectively.

The Hoyle Pond volcanic rocks are geochemicaly similar to the Hersey Lake and Central Formations (Fig. 3B). They have similar immobile element chemistry, specifically TiO_2/Al_2O_3 and Zr/Al_2O_3 ratios indicating that the south volcanic package has very similar geochemistry to the Central Formation (Fig. 8A-D), whereas the north and central volcanic packages correlate with the Hersey Lake Formation (Fig. 9A-D).

Other lithologic units

Younger quartz-feldspar porphyries and quartz porphyries sericite schist cut the south volcanic package. The quartz porphyries are 2- to 4-m-thick, 200-m-long, sericitized and foliated sill composed of ~5 vol percent quartz phenocrysts with rare fuchsitic clasts. The quartz porphyries are intersected by dominant S_3 fabric and folded by D_4. In thin section, the quartz phenocrysts have an embayed dissolution texture typical of felsic extrusions or shallow intrusions. It has a U-Pb zircon age of 2687.6 ± 2.2 Ma (Ayer et al., 2005).

The quartz-feldspar porphyries cut across stratigraphy. They are moderately foliated by S_4 and they have very weak to no metamorphic halos. They are composed of 30 to 40 vol percent albite phenocrysts (5 mm to 1.5 cm) and ~5 vol percent quartz phenocrysts varying in size from 2 to 5 mm within a matrix composed of very fine grained quartz, albite, and muscovite. They have a trachytic texture defined by an alignment of feldspar phenocrysts. Zircons extracted from a sample from the 620-m level returned a U-Pb crystallization age of 2684.4 ± 1.9 Ma, but the sample also contains inherited zircon with an age of 2695.1 ± 3.3 Ma (Ayer et al., 2005).

The quartz-feldspar porphyry and the quartz porphyry have very similar compositions. The two porphyries have identical chondrite-normalized REE patterns, with LREE (18–25 times chondrite) to IREE negative slope and IREE to HREE flat pattern (1 times chondrite; Fig. 7F).

Structure

The mine stratigraphy consists of a south-facing homoclinal sequence of stacked volcanic rocks, previously interpreted to be an anticlinal fold cored by ultramafic volcanic rocks. The volcanic rocks are foliated by a dominant S_3 fabric (Fig. 10A) parallel to bedding that strikes generally eastward. When compared to the deformation history in the rest of the Porcupine gold camp, the Hoyle Pond mine main fabric (S_3) is comparable to what Bateman et al. (2005) describes as S_2. If correct, the S_3 fabric of Bateman et al. (2005) is not observed at the mine (see Table 1) and is restricted to the Porcupine-Destor deformation zone. S_3 of this study is refolded at the mine scale by D_4. The S_4 fabric trends ~070° and is axial planar to isoclinal F_4 folds (Fig. 2) in the 1060 fault zone and to Z-shaped F_4 folds, northwest of the 1060 fault zone (see Figs. 2, 10B). The timing of the D_3 event in this study is constrained between 2687.6 ± 2.2 and 2684.4 ± 1.9 Ma, based on

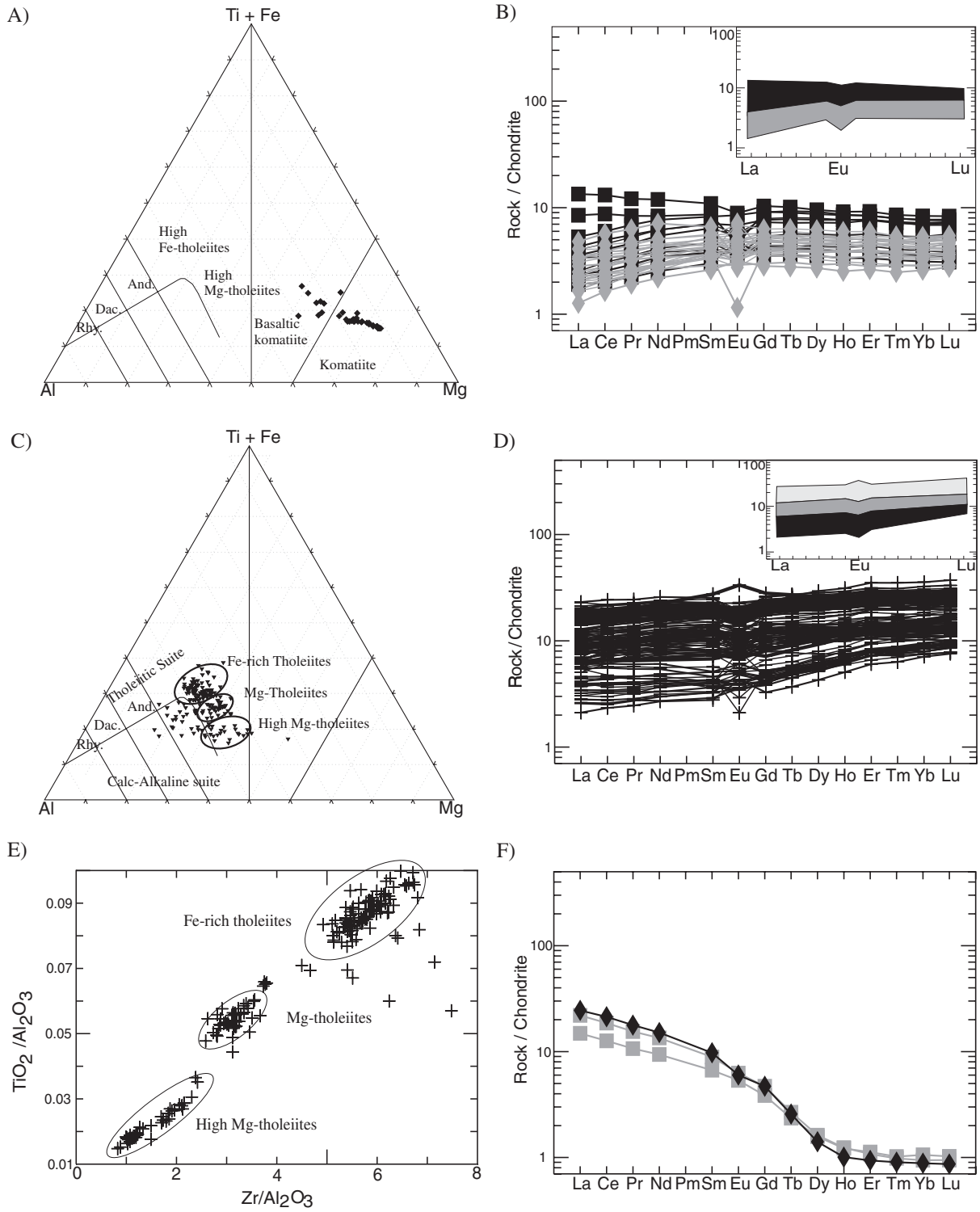

FIG. 7. A. Jensen cation plot (Jensen, 1976) of the central volcanic package volcanic rocks, komatiites, and basaltic komatiites. B. Chondrite-normalized REE pattern of the central volcanic package volcanic rocks, komatiites, and basaltic komatiites. The inset shows the approximate range of the normalized REE abundance of the komatiites (gray) and basaltic komatiites (black). C. Jensen cation plot (Jensen, 1976) of the south volcanic package volcanic rocks, Fe-rich tholeiitic basalts, Mg tholeiitic basalts, and high Mg tholeiitic basalts. D. Chondrite-normalized REE pattern of the south volcanic package volcanic rocks, Fe-rich tholeiitic basalts, Mg tholeiitic basalts, and high Mg tholeiitic basalts. The inset shows the approximate range of the normalized REE abundance of the Fe-rich tholeiitic basalts (pale-gray), Mg tholeiitic basalts (gray), and high Mg tholeiitic basalts (black). E. TiO_2/Al_2O_3 vs. Zr/Al_2O_3, differentiating the three volcanic rock types, Fe-rich tholeiitic basalts, Mg tholeiitic basalts, and high Mg tholeiitic basalts of the south volcanic package. F. Chondrite-normalized REE pattern of the felsic intrusive quartz-feldspar (squares) and quartz (diamonds) porphyry.

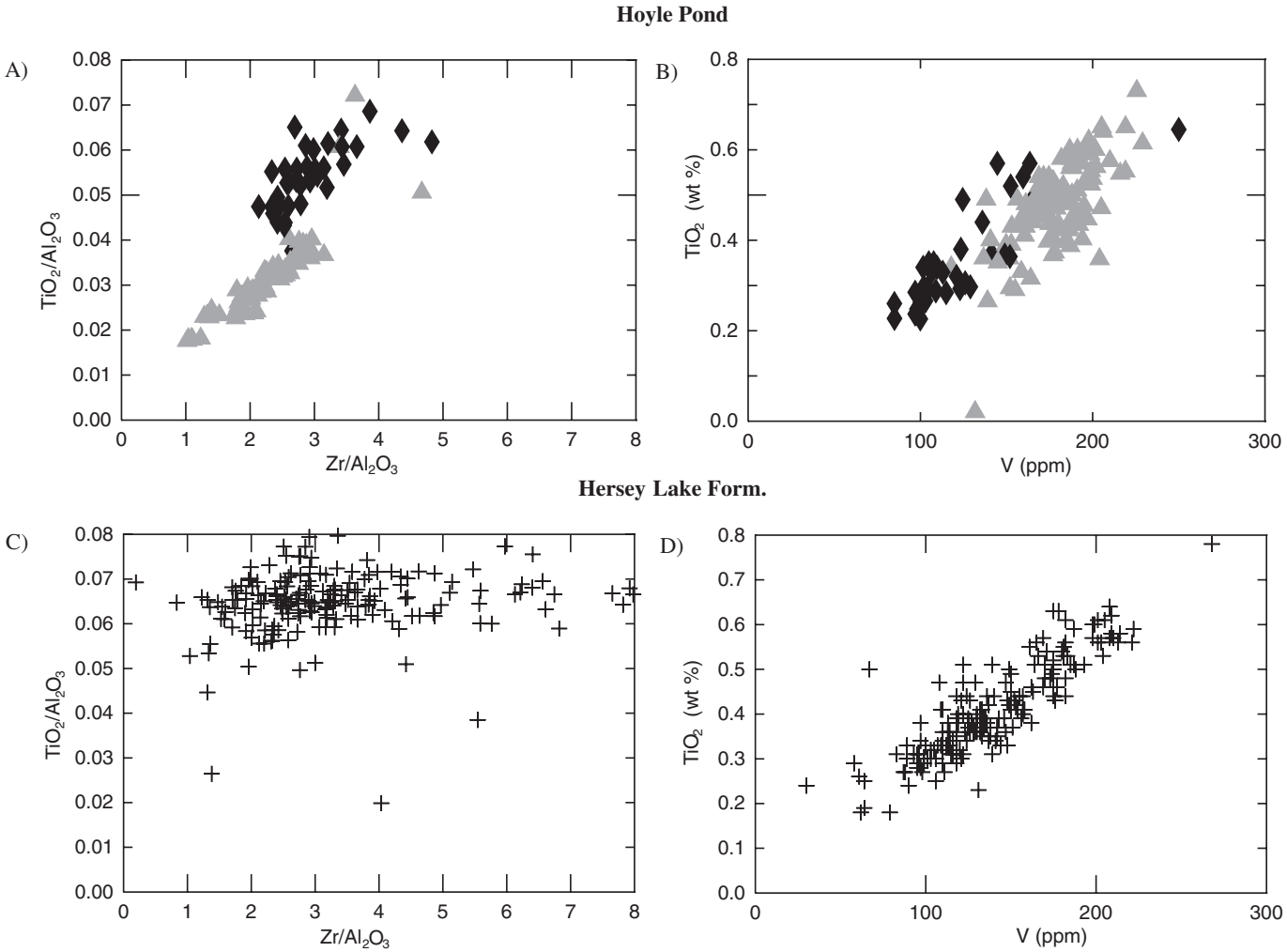

FIG. 8. Comparison of immobile element concentrations in the north volcanic package (triangle) and central volcanic package (diamonds) at the Hoyle Pond mine (A) and (B) to samples of the Hersey Lake Formation of the Tisdale assemblage (C) and (D). A. TiO_2/Al_2O_3 vs. Zr/Al_2O_3 plot of the north and central volcanic packages. B. TiO_2 vs. V plot of the north and central volcanic packages. C. TiO_2/Al_2O_3 vs. Zr/Al_2O_3 plot of the Hersey Lake Formation. D. TiO_2 vs. V plot of the Hersey Lake Formation. A geochemical database was provided by the Porcupine Joint Venture (Goldcorp). The database contains more than 1,000 analyses from samples collected in the Porcupine gold camp. Approximately 200 analyses out of the 1,000 characterize the geochemistry of the Hersey Lake Formation of the Tisdale assemblage.

a crosscutting relationship of S_3 and S_4 with the quartz-feldspar porphyries and quartz porphyries. The quartz porphyries are pre-D_3 and are foliated by S_3; the quartz-feldspar porphyries are post-D_3 and pre-D_4, because they lack the penetrative S_3 fabric, yet possess the S_4 fabric. The loci of mineralization in the 1060 fault zone are coincident with the contacts of the various lithologic units on the limbs of the isoclinal F_4 folds. The 1060 shear zone is a corridor of intense deformation, where S_4, oriented ~070°, is very penetrative and acted as a shear foliation.

Vein descriptions

Both extensional and fault-fill veins are observed at Hoyle Pond. The extensional veins are straight to S shaped, cut across the S_3 and S_4 foliations at high angles, and have a general sinistral rotation. They are generally massive and composed of white to grayish quartz, with local pyrite along the wall rock-vein contact. Locally, some extension veins have a black appearance due to graphite and tourmaline-filled fractures. The fault-fill veins are generally oriented ~070° and have a more diverse mineralogy consisting of massive white to gray quartz, with interstitial tourmaline and/or stylolitic chlorite and, locally, muscovite or Cr muscovite. Other fault-fill veins are mainly composed of massive white quartz and are commonly associated with variable concentrations of graphite in the wall-rock selvages. In the north volcanic package, the fault-fill veins (e.g., 16 vein) are parallel to S_3; however, in the south volcanic package, the fault-fill veins are parallel to S_4.

Gold mineralization

Fault-fill and extensional veins contain free gold flakes ranging from micron to 2-cm size found along stylolites in the veins or randomly distributed in massive veins as millimeter to centimeter gold veinlets.

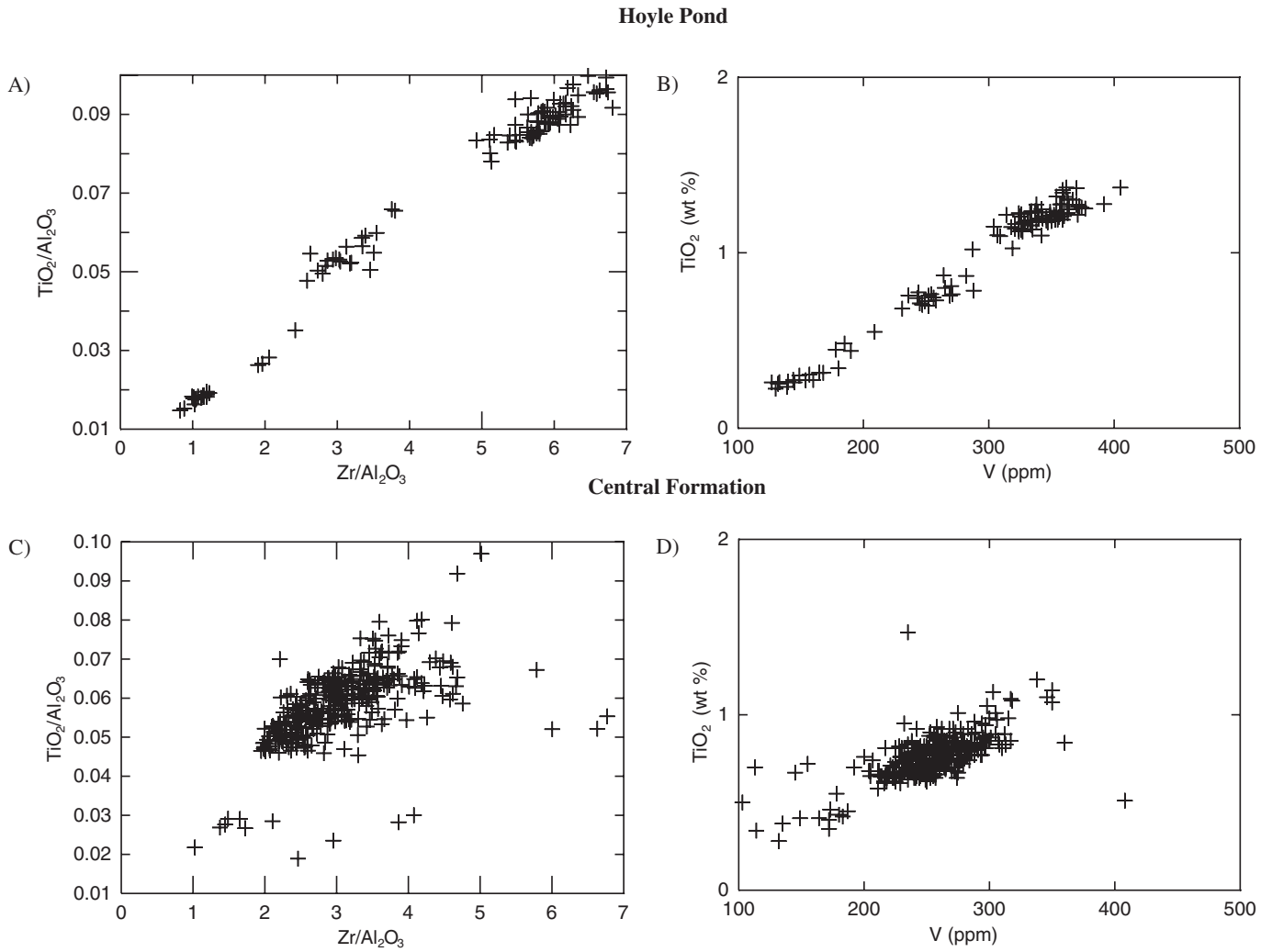

FIG. 9. Trace element comparison of the south volcanic package at the Hoyle Pond mine (A) and (B) with the Central Formation of the Tisdale assemblage (C) and (D). A. TiO_2/Al_2O_3 vs. Zr/Al_2O_3 plot of the south volcanic package. B. TiO_2 vs. V plot of the south volcanic package. C. TiO_2/Al_2O_3 vs. Zr/Al_2O_3 plot of the Central Formation. D. TiO_2 vs. V plot of the Central Formation. A geochemical database was provided by the Porcupine Joint Venture. The database contains more than 1,000 analyses from samples collected in the Porcupine gold camp. Approximately 150 analyses out of the 1,000 characterize the geochemistry of the Central Formation of the Tisdale assemblage.

Alteration

Mapping and sampling of alteration was conducted along three traverses that intersect the B1N, B1, and B3 veins on the 720-m level. The alteration mineral formation appears to have been synchronous with vein development and gold mineralization as indicated by alteration halos which envelop but do not intersect the veins. Three alteration zones were identified, mapped, and sampled: an inner sericite zone surrounding the veins, an outer albite zone, and a graphitic alteration zone (gray zone). The alteration minerals are sericite, fuchsite (Cr muscovite), K-feldspar, albite, carbonates, graphite, chlorite, tourmaline, pyrite, and arsenopyrite. In general, carbonate alteration is pervasive and observed throughout the mine. The intensity of carbonate, sericite, and "fuchsite" alteration increases locally and is best developed in the 1060 fault zone in the vicinity of veins.

The sequence of deformation, alteration and mineralization events is shown in Figure 11A and B. The albite and carbonate porphyroblasts present in microlithons are dissected by a cleavage defined by muscovite and Cr muscovite, with minor quartz and graphite (Fig. 12A), thus demonstrating the existence of early albite and carbonate alteration. Graphite alteration is visible in fault-fill and extension veins, in former wall-rock interstices (Fig. 12B), within flow top breccias and hyaloclastite, and along stylolites and cleavages. Tourmaline is present in stylolites and in the fault-fill veins and extensional veins as coarse euhedral grains. Needles of arsenopyrite occur in the veins and in their wall rocks, which also contain pyrite at vein contacts.

Isocon diagrams show that dilution of immobile elements occurred due to flooding by hydrothermal minerals (Fig. 4C-G; shifting the isocon). K_2O, Na_2O, Cr_2O_3, Rb, CO_2, CaO,

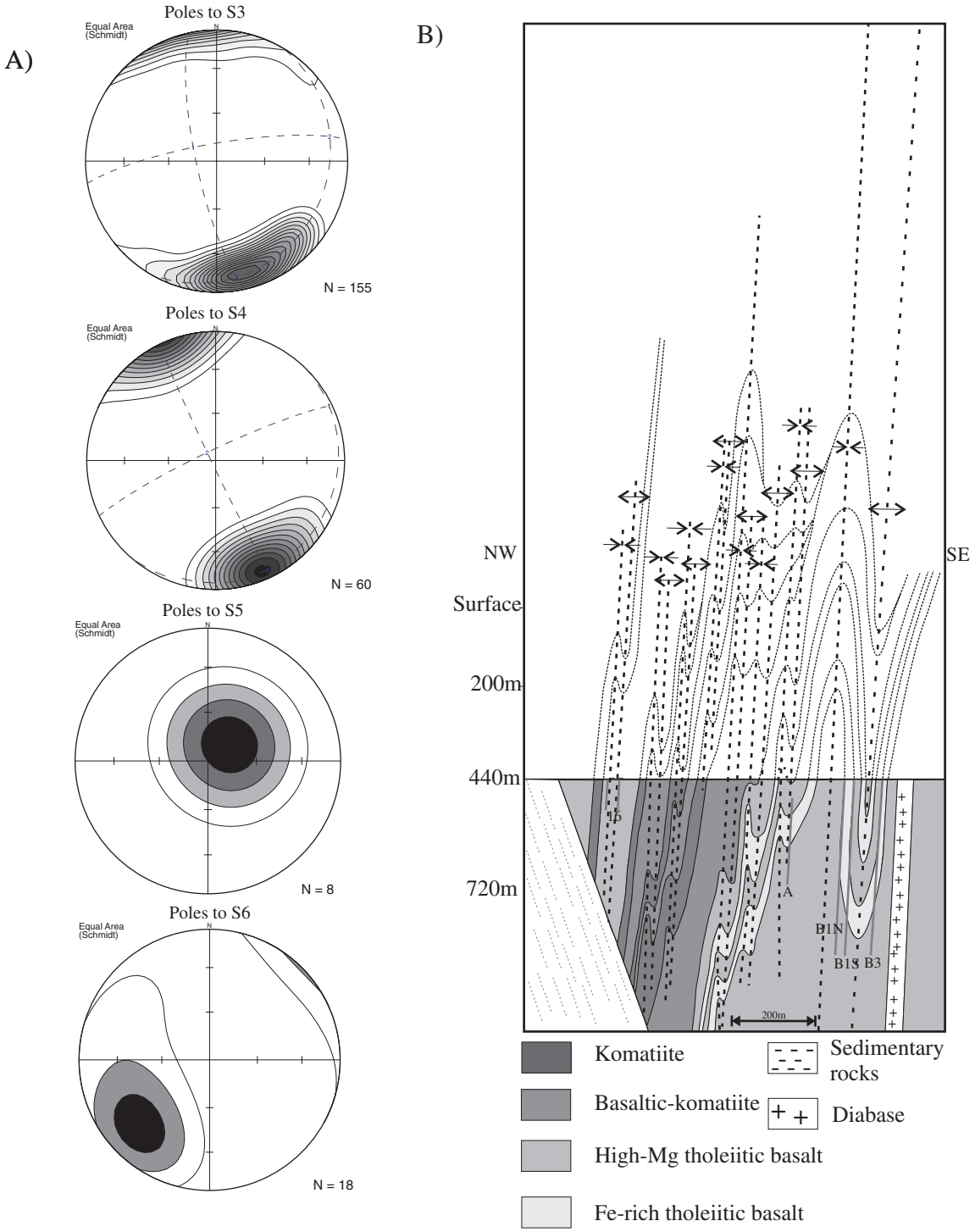

FIG. 10. A. Lower hemisphere equal area projections of poles to S_3, S_4, S_5, and S_6, measured on the 400- (3 level), 440-, 720-, and 880-m level at the Hoyle Pond mine. B. Vertical section of Hoyle Pond mine along a northwest-southeast section with projection of F_4 folds to and above surface.

Eu, FeO, MgO, and to a minor extent La (LREE), were all mobile to varying degrees.

Sericite alteration zone

The sericite alteration zone consists of muscovite, Cr muscovite, calcite, dolomite, and ferroan dolomite and graphite, plus microcrystalline alkali feldspar, local acicular arsenopyrite and anhedral to euhedral pyrite. Typically, the sericite zones extend 4 to 6 m from the veins and range in color from pale gray, to light beige, to light yellow, and possess a weak to strong pale gray sericitic cleavage (S_3 and/or S_4). The extent of the alteration appears to be dependent on the host-rock

TABLE 1. Comparison of the Chronology of Deformation Events in the Porcupine Gold Camp from Different Authors

Rhys (2003b)			Bateman et al. (2005)		Dinel et al. (this study)	
Age (Ma)	Lithologic units	Deformation events	Age (Ma)	Lithologic units	Deformation events	Deformation events
2730–2725	Deposition of the Deloro assemblage		2730–2723	Deposition of the Deloro assemblage		
2708–2700	Deposition of the Tisdale assemblage		2708–2703	Deposition of the Tisdale assemblage		
2700–~2690		D_{1a} : northwest-trending folds, no foliation developed or preserved			D_1: extensional-uplift event, no foliation associated; Tisdale-Porcupine unconformity	D_1 : no fabric observed at the mine
~2691–~2680	Deposition of the Porcupine assemblage		2691–~2682	Deposition of the Porcupine assemblage	D_2: isoclinal folds (e.g. North Tisdale anticline, Porcupine syncline) and late thrust event (Tisdale thrust over Porcupine); early dip-slip faulting in the Destor-Porcupine deformation zone	D_2: no fabric observed at the mine (based on Rhys, 2003a, internal company report)[1]
~2680–~2675		D_{1b}: west-northwest-trending isoclinal folds lacking axial planar cleavage, modification of D_{1a} folds				D_3: east-west isoclinal folds with axial planar cleavage parallel to bedding, possible late gold mineralization (2687 > D_3 >2684), late D_3 thrust, Tisdale on Porcupine
~2675–~2672		Destor-Porcupine fault system, early faulting, >10 km sinistral strike-slip displacement, north side down	2678–2669	Deposition of the Timiskaming assemblage and albitite dike at the McIntyre mine (~2672 Ma)	D_3: folding (e.g. South Tisdale anticline) and axial planar cleavage S_3 dominant penetrative fabric in Timmins (oriented 281°) post-677Ma, result of oblique-slip movement along major deformation zones; gold minerlization associated with D_3	
~2674–~2672	Deposition of the Timiskaming assemblage and albitite dike		> 2669		Formation of the Dome fault; D_4: isoclinal folding and S_4 axial planar cleavage oriented 070°, restricted to the Timiskaming syncline, dip-slip movement associated with D_4 faults and gold mineralization	D_4: penetrative S_4 fabric oriented 070°, axial planar to isoclinal folds and gold mineralization associated with D_4
~2672–(?)		D_2 + regional metamorphism, penetrative S_2; east-southeast cleavage, late gold mineralization			D_5: constrictional strain, observed west of Porcupine syncline, forming very stretched pillows, prominent where the Destor-Porcupine fault deflects; D_6: flat-lying crenulation cleavage	D_5: northeast crenulation cleavage associated with small-cale Z folds and conjugate kinks; D_6: sub-horizontal crenulation cleavage axial planar to broad open fold (vertical displacement along S_4)
		D_3: spaced S_3 foliation east-southeast cleavage, continuation of sinistral displacement; D_4: late retrograde deformation, north-northeast crenulation cleavage and conjugate kinks; D_5: shallow southwest-dipping crenulation cleavage			D_7: north-northeast-striking kink and chevron folds, steeply dipping axial planar cleavage	

[1] Rhys (2003b), Structural style and setting of gold deposits, Hollinger-McIntyre to Pamour, Porcupine mining camp: A Field trip guide for Placer Dome exploration seminar, October 1, 2003, 45 p.

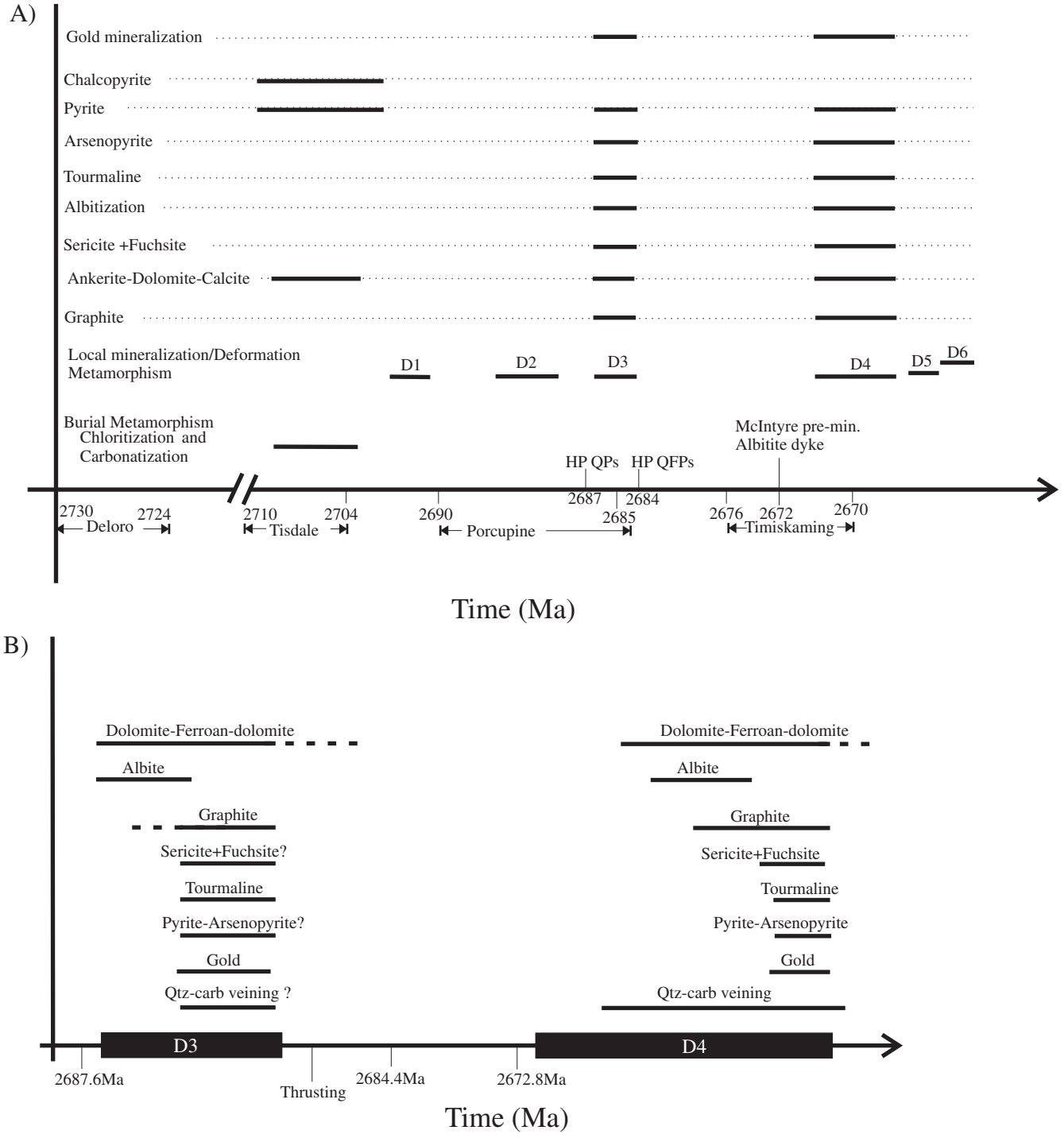

FIG. 11. A. Paragenetic sequence of deformation, alteration, and mineralization vs. time in the Porcupine gold camp based on Bateman et al. (2005) and field observation at the Hoyle Pond mine. B. Paragenetic alteration sequence at the Hoyle Pond mine.

composition, as the most significant enrichment in mobile elements is in high Mg tholeiitic basalts. K_2O, Rb, As, and S concentrations increase adjacent to veins (Fig. 13B, C). The enrichment in Rb is identical to that of K_2O (Fig. 4D, E) and reflects a substitution of K by Rb in the crystal lattice of sericite and alkali feldspars. Sericitic alteration and element enrichment and depletion also can be observed at lithologic contacts where no veins are present.

Chromium enrichment

Chromium content increases in close proximity to veins and is found in muscovite and Cr micas (Table 2), replacing Al in

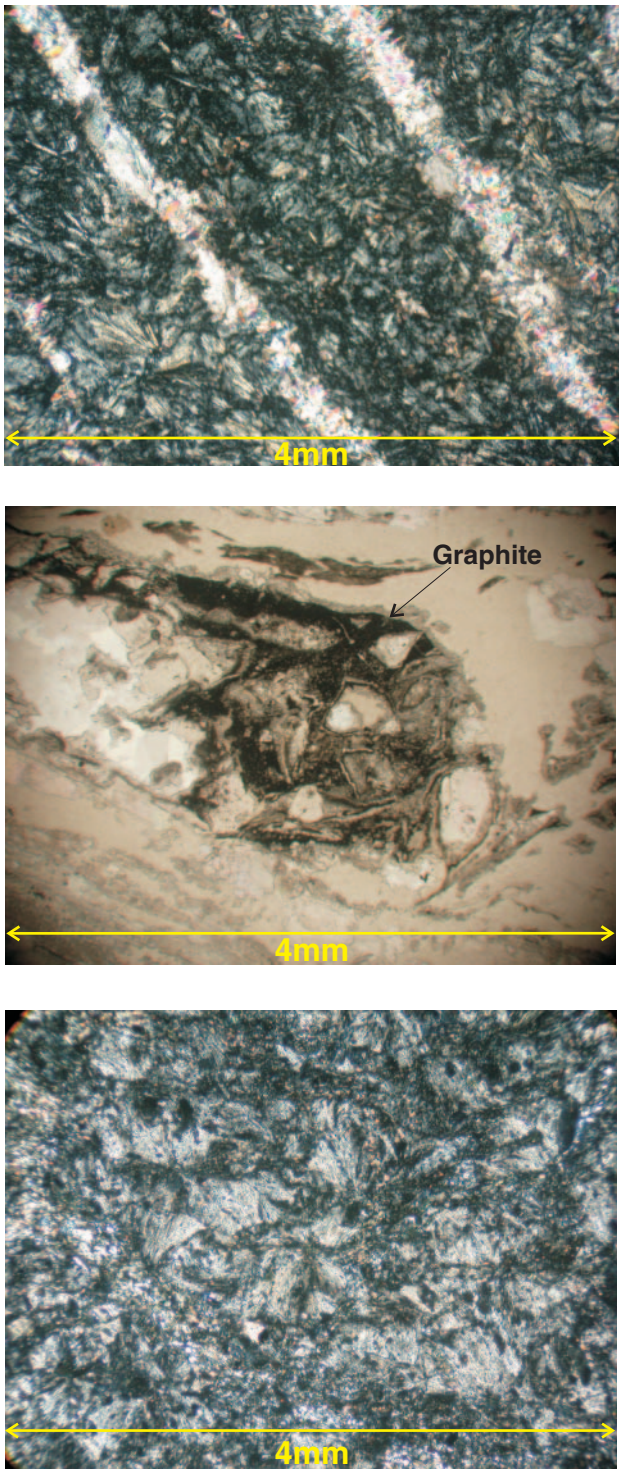

FIG. 12. A. Spherulitic textures in albitized microlithons cut by S_4 cleavage containing muscovite, Cr muscovite, and Fe dolomite, crossed polars B. Graphite alteration in zone of increased porosity in a brecciated clast, natural light. C. Secondary spherulitic albite overprinting earlier chlorite (black), crossed polars.

the octahedral site of the crystal lattice (Deer et al., 1992). Chromium contents in tholeiitic basalts of the area are generally 150 to 250 ppm, similar to oceanic crust (Faure, 1998). In proximity to the quartz-carbonate gold bearing veins, chromium concentrations increase by a factor of 6 to reach levels of 1,200 ppm. We note that the nickel concentration and the Mg number do not follow the chromium trend, indicating that the chromium enrichment is not a primary igneous feature. Moreover the isocon diagrams (Fig. 4D, E) clearly show Cr enrichment. Moritz and Crocket (1991) and McCuaig and Kerrich (1998) also noted fuchsite-rich quartz veins at the Dome mine in Timmins and suggested that Cr could be mobile.

Albite alteration zone

These zones envelop the sericite alteration and are best observed in thin section. The albitized rock consists of a fine-grained apple-green groundmass with albite porphyroblasts and spherulitic secondary albite overgrowing chlorite (Fig. 12C). Chondrite-normalized patterns (e.g., Fig. 6B) of albitized rocks have negative Eu anomalies that are likely due to the loss of Ca and Eu in the transformation of Ca plagioclase to albite (e.g., Fowler and Doig, 1983). The Na enrichment decreases approaching the vein and is replaced by an increase in K_2O as sericite alteration. The albite alteration zones can be difficult to identify due to the number of overlapping alteration halos around veins and the fact that mineralization is dominated by sericitic alteration.

Graphitic alteration ("gray zone")

Gray zone alteration trends roughly 070° and commonly cuts across the stratigraphy (Fig. 2) parallel to the sericite and albite alteration zones. The gray zones extend for several hundred meters along strike and range from 0.5 to 20 m in thickness. This alteration is commonly centered and does not intersect the quartz-carbonate veins. It is associated with coarse brecciation and a modal increase in graphite, pyrite (including globular pyrite), calcite, dolomite, and ferroan dolomite. Drilling shows that the gray zones form anastamosing three-dimensional networks surrounding lenses of less altered rock (Rye, 1987). They are commonly spatially associated with Au-rich quartz veins. In the 1060 fault zone, the graphite enrichment is found in the vicinity of veins and correlates with the zone of intensive shear mapped by D. Rhys (unpub. report for Porcupine Joint Venture, 2003, 36 p.).

Previous workers (Downes et al., 1984; Rye, 1987) have suggested that the graphite was formed from organic carbon. Downes et al. (1984) reported gas chromatograph analyses of samples, which showed peaks corresponding to C-H bonds as well as toluene and xylene structures; this indicated the presence of highly condensed aromatic polymers. Hodges (1982) showed that 22 percent of reduced carbonaceous material at Owl Creek is organic. For this study, we collected samples from the graphitic shear on the 440-m level and the graphitic alteration enveloping the 16 vein on the 440-m level, and analyzed them for ^{13}C concentration. The $\delta^{13}C$ values are in the range of –24 to –27 per mil. The abundance of isotopically light carbon could indicate an organic source or fractionation of either mantle or atmospheric C. Ultraviolet absorption spectra of the graphite showed a strong absorption peak at

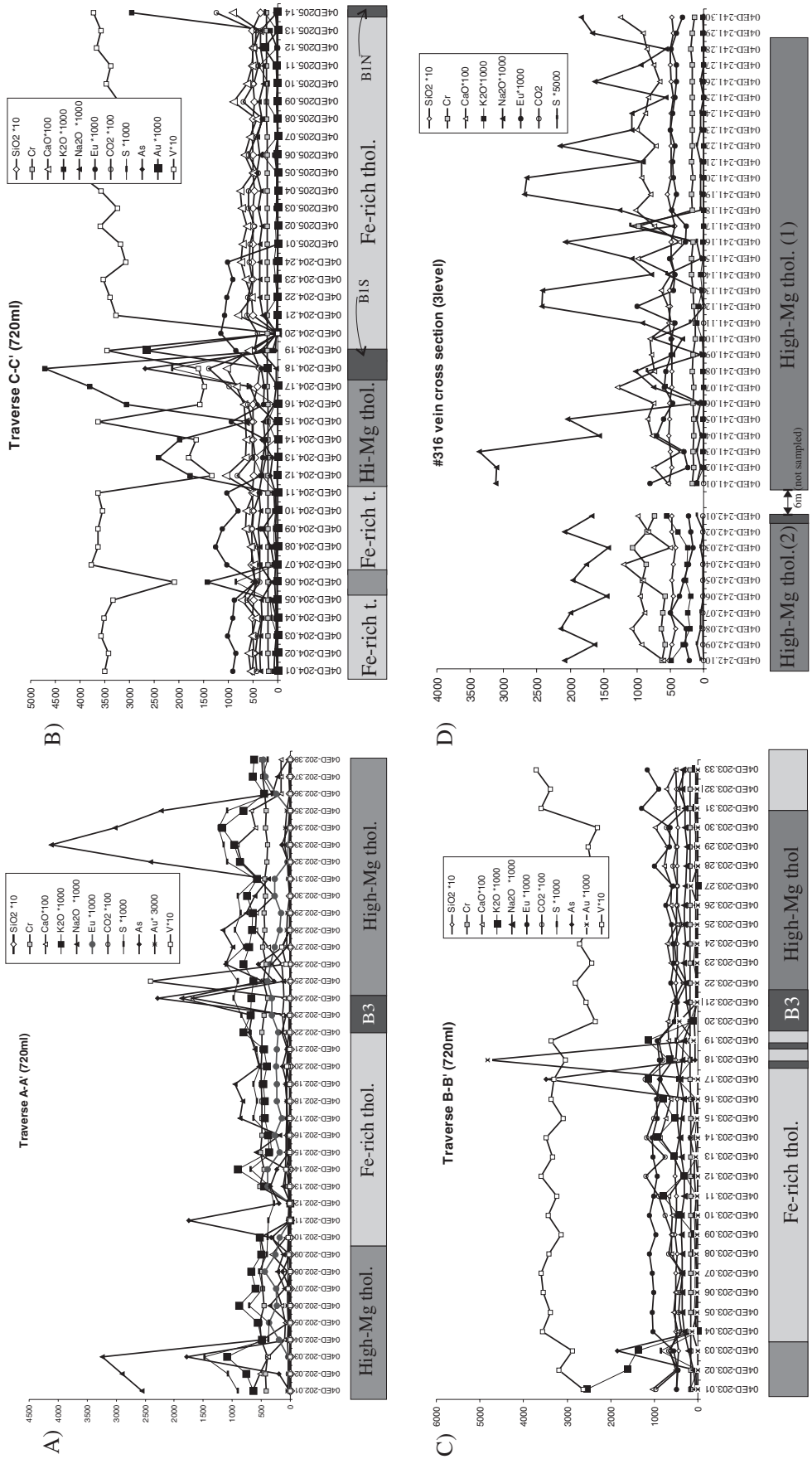

FIG. 13. Scaled enrichment and depletion plot of trace and major elements along three traverses (A-A', B-B', C-C') on the 720-m level. The traverses cut across the stratigraphy folded by F_4 along the 1060 fault zone. A fourth traverse cuts across the 3 level (16 vein). Samples along the four traverses were taken at 1-m intervals. SiO_2 = wt % × 10, Cr = ppm, CaO = wt % × 100, K_2O = wt % × 1,000, Na_2O = wt % × 1,000, Eu = ppm × 1,000, CO_2 = wt % × 100, S = wt % × 1,000, As = ppm, Au = ppm × 1,000, and V = ppm × 10.

TABLE 2. Electron Microprobe Data for Carbonate and Cr Muscovite (major oxide expressed in wt %)

Carbonate

Sample no.	203-17-1	203-17-3	203-17-6	203-17-7	204-07-1	204-07-3	204-07-4	70-1	70-2	70-4	77-1-2	204.05-2-1
CaO	28.75	28.95	28.56	27.5	56.33	57.87	55.65	56.34	57.97	57.53	57.46	57.11
FeO	17.36	17.62	18.75	17.19	0.99	0.92	0.88	0.38	0.02	0.09	0.96	1.13
MnO	0.35	0.46	0.42	0.4	1.02	0.92	0.99	1.72	0.07	0.09	0.53	0.68
MgO	10.33	10.15	8.88	9.75	0.41	0.41	0.37	0.23	n.d.	n.d.	0.37	0.39
SrO	0.01	0.02	n.d.	n.d.	0.04	n.d.	n.d.	n.d.	n.d.	n.d.	n.d.	n.d.
BaO	n.d.	0.1	n.d.	0.1	0.07	0.08	0.01	0.05	n.d.	n.d.	n.d.	0.02
CR_2O_3	0.03	0.02	0.02	0.02	0.02	0.03	0.03	0.03	0.03	0.03	0.03	0.03
Total	56.83	57.32	56.63	54.96	58.88	60.23	57.93	58.75	58.09	57.74	59.35	59.36

Cr muscovite

Sample no.	115-01-1	115-01-2	115-01-3	115-01-4	115-01-5	115-02-1	115-02-2	115-03-1	115-04-1	115-04-1	115-04-2	115-04-3
SiO_2	48.49	48.07	48.42	47.76	48.34	48.17	48.42	48.28	48	48.75	48.04	48.66
Al_2O_3	32.59	32.78	32.99	33.46	30.91	31.85	32.39	32.25	32.77	32.88	32.58	31.88
TiO_2	0.36	0.34	0.4	0.38	0.34	0.37	0.43	0.22	0.34	0.37	0.32	0.35
Cr_2O_3	1.19	1.18	0.52	1.45	2.77	1.92	1.71	1.97	1.54	1.59	0.98	1.77
V_2O_3	0.09	0.09	0.12	0.08	0.11	0.09	0.09	0.06	0.07	0.09	0.1	0.09
FeO	0.9	0.77	0.96	0.86	0.92	0.99	1	0.97	0.92	1.02	1.23	1.17
MgO	1.63	1.48	1.48	1.29	1.55	1.6	1.51	1.52	1.45	1.5	1.54	1.61
MnO	0.02	0.03	0.02	n.d.	n.d.	n.d.	n.d.	0.03	n.d.	n.d.	n.d.	0.03
K_2O	10.82	10.78	10.74	10.67	10.77	10.8	10.85	10.55	10.83	9.81	10.68	10.82
CaO	n.d.	n.d.	n.d.	0.02	0.02	n.d.	0.01	0.01	0.01	n.d.	0.05	0.03
Na_2O	0.29	0.32	0.28	0.37	0.29	0.24	0.29	0.35	0.4	0.29	0.38	0.3
BaO	0.19	0.26	0.2	0.33	0.23	0.23	0.19	0.29	0.26	0.26	0.22	0.26
Cl	0.01	0.01	n.d.	n.d.	n.d.	n.d.	n.d.	n.d.	n.d.	n.d.	n.d.	n.d.
F	n.d.	n.d.	0.15	0.11	0.17	0.1	0.07	0.09	0.1	0.11	0.11	0.09
Total	96.58	96.11	96.28	96.78	96.42	96.36	96.96	96.59	96.69	96.67	96.23	97.06

Sample no.	115-04-4	119-01-1	119-01-2	119-01-3	119-02-0	119-02-3	119-03-1	119-03-2	119-03-3	119-04-1	119-04-2	119-04-3
SiO_2	48.18	47.93	48.19	48.01	48.02	48.01	47.76	48.3	47.62	47.78	47.37	48.31
Al_2O_3	33.2	34.79	34.91	35.52	33.34	33.7	34.08	32.89	32.3	35.8	34.78	35.97
TiO_2	0.32	0.18	0.15	0.11	0.25	0.3	0.22	0.26	0.23	0.09	0.21	0.15
Cr_2O_3	0.93	1.17	1.11	1.01	1.33	1.22	1.91	1.99	2.29	0.33	0.87	0.9
V_2O_3	0.09	0.12	0.1	0.12	0.1	0.13	0.07	0.1	0.06	0.11	0.08	0.1
FeO	0.78	0.6	0.55	0.44	0.86	0.82	0.58	0.74	0.75	0.39	0.63	0.43
MgO	1.43	0.95	0.93	0.68	1.26	1.39	0.97	1.31	1.2	0.8	0.99	0.69
MnO	n.d.	n.d.	0.04	0.01	0.04	n.d.	0.01	n.d.	n.d.	n.d.	0.03	n.d.
K_2O	10.72	10.02	10.24	10.04	10.46	10.19	10.38	10.19	10.08	10.03	9.82	9.18
CaO	n.d.	0.01	0.03	0.01	0.09	n.d.	n.d.	0.01	0.06	0.09	0.46	0.03
Na_2O	0.34	0.51	0.38	0.53	0.49	0.41	0.5	0.4	0.48	0.49	0.6	0.58
BaO	0.29	0.14	0.13	0.16	0.28	0.19	0.17	0.12	0.19	0.11	0.12	0.14
Cl	n.d.	n.d.	n.d.	n.d.	n.d.	0.01	0.01	0.03	0.01	0.01	0.01	0.02
F	0.06	0.08	0.07	0.11	0.08	0.06	0.09	0.13	0.12	0.25	0.02	0.07
Total	96.34	96.5	96.83	96.75	96.6	96.43	96.75	96.47	95.39	96.28	95.99	96.57

Sample no.	116A-1-1	116A-1-2	116A-2-1	116A-2-2
SiO_2	48.79	48.55	49.61	48.49
Al_2O_3	31.73	31.1	31.51	33.26
TiO_2	0.25	0.39	0.41	0.18
Cr_2O_3	1.41	1.49	1.4	1.03
V_2O_3	0.07	0.05	0.03	0.07
FeO	0.67	0.83	0.71	0.64
MgO	1.56	1.9	1.89	1.25
MnO	n.d.	0.03	n.d.	n.d.
K_2O	10.45	10.57	10.78	10.57
CaO	n.d.	n.d.	n.d.	0.03
Na_2O	0.25	0.23	0.23	0.22
BaO	0.17	0.12	0.07	0.13
Cl	n.d.	n.d.	n.d.	n.d.
F	0.08	0.14	0.14	0.21
Total	95.43	95.4	96.78	96.08

280 nm (Fig. 14), indicating the presence of lignoid molecules (Farmer and Morrison, 1960; Sapek et al., 1980).

The graphite in the graphitic shear has a similar chemical signature to that of the gray zone.

Carbonate alteration

The carbonate alteration is developed beyond the mine area. Two types of carbonate alteration are observed, an early one consisting of deformed calcite crystals in amygdules and pillow selvages and a later one consisting of porphyroblasts of dolomite and ferroan dolomite. Figure 13 documents a significant enrichment in CO_2 in the Mg-rich rocks of the 1060 fault zone in comparison to the Fe-rich tholeiitic basalts.

Silica alteration

Silica alteration is observed in thin section as stringers and patches of anhedral quartz and resulted in the dilution of immobile elements (Fig. 4C). This alteration is less evident in the Fe-rich tholeiitic basalts than in the Mg-rich volcanic rocks.

To explore the geochemical data more fully, a principal components analysis was carried out (Dinel, 2007). Analysis of mobile element shows that K_2O, Cr, and SiO_2 covary as expected for the sericite alteration zones. Similar covariance in CaO and Na_2O defines the albite alterations zones. A principal components analysis of immobile element concentrations confirms the classification of the rocks into Fe-rich and high Mg groupings.

Discussion

The vein systems at Hoyle Pond (e.g., 1060 fault zone) were emplaced at contacts between different rock units. Similarly in the Hollinger and McIntyre system, Melnik-Proud (1992) and Brisbin (1997) observed that a majority of veins were located at flow contacts. This raises the possibility that units with high primary porosity, such as interstices in flow breccias, could have been preferred hosts for hydrothermal mineralization. Alternatively porosity may have been developed at contacts during faulting or shearing as a result of the competency contrast between adjacent units. The alteration patterns observed at the Hoyle Pond mine are consistent with those at the Hollinger-McIntyre deposit (Melnik-Proud, 1992; Brisbin, 1997) and in many other Archean gold deposits (Robert, 2001). At Hoyle Pond, the Au mineralization is hosted in D_3 and D_4 structures, indicating the existence of pre- and post-Timiskaming assemblage Au mineralization. We have no evidence to constrain the end of D_4, but F_4 folds and associated fabric (S_4) are found within Timiskaming sedimentary units with a maximum depositional age of 2670 Ma (Ayer et al., 2005).

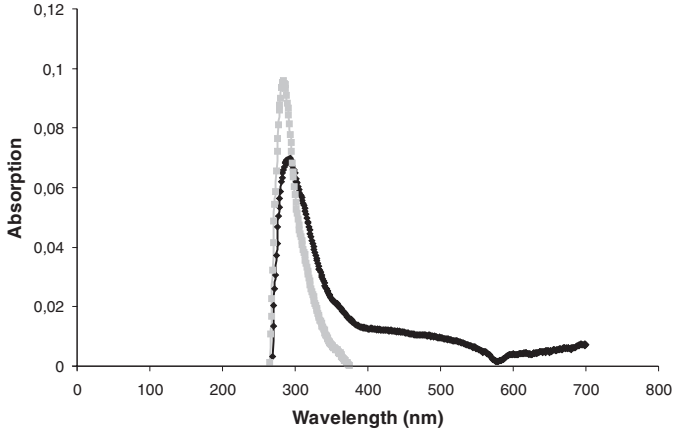

FIG. 14. A. Ultraviolet absorption spectrophotometry (which measures the absorption of light) plot for graphitic material samples of the graphitic shear on the 440-m level and the gray zone alteration on the 720-m level. The structure of the molecules determines the degree and wavelength of the absorption.

Regionally, Au-bearing quartz veins in the Timmins area are parallel to a prominent 070° fabric, which may suggest that the two are related. At Hoyle Pond, this fabric does not intersect Au-bearing quartz veins and the boudinage of the veins is interpreted to have formed as part of the shear-veining process associated with D_4. Across the Timmins area it is difficult to decipher the timing of the various generations of fabrics because they do not have a constant dip, hence fabrics having the same strike but opposing dips in adjacent outcrops may have been interpreted as the result of different deformation events. These structural complications are an ongoing problem that still needs to be resolved.

The dominant foliation (S_3) formed during north-south compression, after the deposition of the Tisdale and Porcupine assemblages. S_2 and S_3 have an average orientation of 075/84 and 281/84, respectively, in the Timmins area (Bateman et al., 2005). At Hoyle Pond, S_3 is subparallel to lithologic contacts and interpreted to be axial planar to F_3 isoclinal folds. The thrust fault observed at the northern contact of the north volcanic package formed late during D_3. Mineralization also began during D_3 as a result of the migration of fluids along the D_3 thrust fault, which resulted in the formation of extensional veins normal to S_3 and fault-fill veins subparallel to S_3 (e.g., 13, 14, 15, 16 veins). However, it is also possible that mineralization in the north volcanic package could have formed during D_4 and filled older D_3 structures. D_4 resulted in localized isoclinal folding and in the formation of a pervasive 070° S_4 foliation containing the majority of the gold-bearing veins in the 1060 fault zone. These fault-fill and extensional veins (e.g., B1, B1N, B1S, B3, UP, etc.) likely formed by flexural shear along the limbs of isoclinal F_4 folds (Fig. 2). Figure 10B illustrates the relationships of F_4 first-order folds with mineralization.

Mineralization in the Hollinger-McIntyre deposits also was syn-D_4 and it overprints an albitite dike dated at 2672.8 ±1.1 Ma (U/Pb zircon: Ayer et al., 2005). We speculate that mineralization at the Hoyle Pond mine was coeval with that of the Hollinger-McIntyre system. We suggest that sedimentary rocks buried during D_3 folding and thrusting were heated and fluids expelled from these rocks migrated along permeable D_3 structures (Fig. 14). These processes were likely repeated during the D_4 event.

Gold mineralization is interpreted to have been coeval with wall-rock alteration. The gold-bearing veins are surrounded by muscovite and Cr muscovite alteration, which in turn is surrounded by albite alteration. The so-called "gray zone" alteration described by Downes et al. (1984) is caused by filling of pores by graphite. The gray zone is centered on the gold-bearing veins, does not intersect the veins, and is interpreted

to be coeval with mineralization. The source of the carbon was most likely organic matter in sedimentary rocks, which also were the source of As and B. Such marine sediments, typically contain significant amounts of As and B (Faure, 1998). The most plausible sedimentary source would have been the Porcupine assemblage rocks surrounding the mine volcanic rock sequence.

The enrichment in Cr (Fig. 4C-E) demonstrates that chromium was mobile during hydrothermal activity. Chromium has two main oxidation states, as a trivalent (Cr^{3+}) or hexavalent ion (Cr^{6+}). Cr^{3+} is immobile, but when oxidized to Cr^{6+} it becomes highly mobile. The oxidation efficiency of Cr^{3+} to Cr^{6+} increases with increasing temperature and pressure in aqueous solutions (Henry, 2000) from 67 percent at 197ºC to 95 percent at 347ºC (Anderson, 1975). The latter temperature is similar to estimated temperatures for auriferous hydrothermal fluids in the Abitibi greenstone belt (e.g., Olivo and Williams-Jones, 2002). Based on the observed correlation of K and Cr in the alteration halos surrounding the veins, we suggest that the association can be explained by the oxidation of Cr^{3+} to Cr^{6+} and transportation in the fluid with K^{+}.

The enrichment of Cr in the wall rock is possibly due to the reduction of Cr^{6+} and reprecipitation of Cr^{3+} in Cr-rich micas. The most efficient reductants are dissolved Fe II ions (Sass and Rai, 1987), Fe^{2+} in sulfides (pyrite), thiol, hydrogen sulfides, and organic matter (Zouboulis et al., 1995; Thornton and Amonette, 1999 Kim et al., 2001; Szulczewski et al., 2001). Thio complexes are often cited as the agents by which gold is transported in hydrothermal solutions that produced many Au deposits (e.g., Seward, 1973; Böhlke, 1989; Ropchan et al., 2002). It seems likely that Cr^{6+} and Au thio complexes and organic matter could not coexist in the same fluid. Therefore, we conclude that more than one fluid was involved and postulate that fluid-mixing processes were responsible for coincident Cr enrichment and Au precipitation at Hoyle Pond. In this model, gold at the Hoyle Pond mine was likely transported as a thio-complex in a fluid that mixed with an oxidizing fluid transporting Cr^{6+}, forming graphite, pyrite, arsenopyrite, tourmaline, muscovite, Cr muscovite, and precipitating gold.

Van Hees et al. (1999) in a study of gold mineralization of the Yellowknife area (NWT, Canada) reported that Fe- and Ti-enriched metavolcanic rocks were preferred hosts for the precipitation of gold, and that metasedimentary rocks were an important conduit and/or source of fluids, metals, and ore-forming constituents. Shelton et al. (2004) proposed, based on stable isotope work, that multiple fluids were responsible for gold mineralization in the Yellowknife area. The interpretation of the oxygen isotope data indicated that fluids emerged from both metasedimentary and metavolcanic rocks but that there was no evidence of fluid mixing.

Conclusions

Geochemical data and facing direction determinations demonstrate that the north and south volcanic packages are not equivalent, indicating that the three volcanic packages represent a south-facing homoclinal sequence, which was previously thought to be an anticline fold cored by ultramafic volcanic rocks. The stacked volcanic rocks at Hoyle Pond correlate with the Hersey Lake and Central Formations of the Tisdale assemblage.

In contrast to the Holloway mine (Ropchan et al. 2002), which is hosted in similar rocks ~100 km to the east of Timmins, there is no correlation between the Fe/Mg ratio of the host rock and gold mineralization at Hoyle Pond (Fig. 15). However, the high Mg tholeiitic basalts are significantly more enriched in mobile elements than Fe-rich tholeiitic basalts suggesting that, in this deposit, the high Mg tholeiitic basalt was more prone to reaction with the hydrothermal fluids.

The mineralizing fluid was injected during isoclinal folding and thrusting associated with D_4 and D_3. Mineralized fault-fill veins were emplaced in shear zones located at lithologic contacts. Two generations of fault-fill veins are present at Hoyle Pond; in the north volcanic package fault-fill veins are hosted in D_3 structures, and in the south volcanic package, more precisely the 1060 fault zone, the fault-fill veins formed during D_4.

Analyses of geochemical data show that the REE, Al, Zr, Ti, and Y were relatively immobile during alteration. The alteration associated with Au-bearing quartz-carbonate veins is zoned and consists of an inner sericite alteration and an outer albite alteration zone. Carbonate alteration is ubiquitous. The sericite alteration zone is composed of muscovite, Cr muscovite ("fuchsite"), quartz, carbonate, arsenopyrite, pyrite, tourmaline, and graphite, with a concomitant enrichment in K_2O, Cr, SiO_2, CO_2, As, and S. The albite alteration zone is composed of albite, quartz, and carbonate, with enrichment in Na_2O, CO_2, and SiO_2.

Cr is significantly enriched proximal to mineralized veins and was likely introduced by an oxidized fluid in the mobile hexavalent state, whereas gold and carbon were likely transported in reduced fluids. Thus it is hypothesized that a reduced C-, B-, As-, Au-bearing fluid mixed with an oxidized fluid carrying Cr, thereby precipitating gold. Trace concentrations of organic matter preserved in graphitic shear and graphite alteration and enrichment of As and B suggests that theses components were derived from a sedimentary source, most likely the subjacent Porcupine assemblage sedimentary rocks. Gold may also have come from the sedimentary rocks.

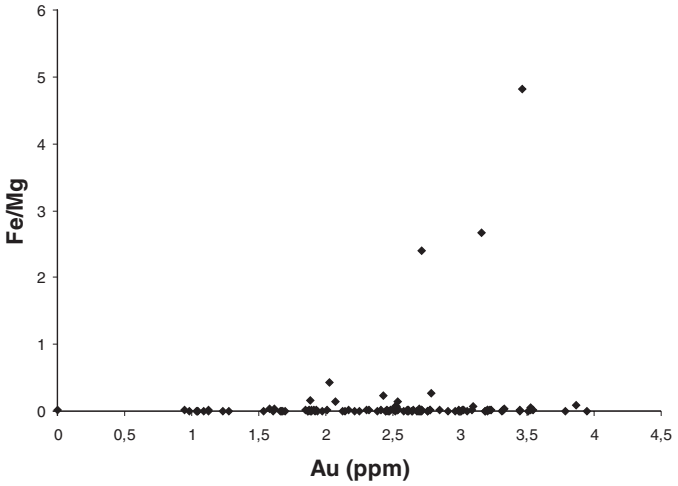

FIG. 15. Plot of bulk Fe/Mg ratio vs. Au content in volcanic rocks of the 1060 fault zone, 720-m level. Note that, with the exception of three points, Au concentration does not increase with Fe/Mg ratios.

We postulate that the Porcupine assemblage sedimentary rocks were transported to depth by burial, folding, and thrusting, and fluids were expelled and migrated along D_3 and D_4 structures (thrust faults; Fig. 16). These reduced fluids were focused into porous and permeable volcanic rocks and mixed with locally derived oxidized Cr-bearing fluids to precipitate gold. Circulation of hydrothermal fluids was reinitiated during D_4. Alternatively, the bulk of the mineralization is syn-D_4 and was locally injected in previously formed D_3 structures.

Acknowledgments

We thank David Rhys for constructive discussions (on outcrops) on the structural evolution of the Hoyle Pond deposits and the Timmins Gold camp. We also acknowledge a fruitful discussion with Howard Poulsen. ED is grateful to Keith Benn for numerous discussions on Archean tectonics. We thank him, Benoit Dubé, Norman Duke, Damien Gaboury, and, in particular, Bruno Lafrance for their insightful reviews that considerably improved the focus and clarity of the manuscript. Ian Clark provided discussion on oxidation reactions in aqueous environments and Henri Dinel on organic geochemistry. The geologic staff of the Porcupine Joint Venture is thanked for providing maps, drill log, training, underground assistance, and their knowledge of the mine.

The Ontario Geological Survey is thanked for providing numerous geochemical analyses. We thank Tito Scaiano and his group in the chemistry department at the University of Ottawa for help with the ultraviolet absorption measurement and also Glenn Facey of the chemistry department for the NMR analysis. Peter Jones (Earth Sciences Dept., Carleton University) provided electron microprobe analysis and Ron Hartree (Earth Sciences Dept., University of Ottawa) provided the XRF analysis. The G.G. Hatch Stable Isotope Laboratory (University of Ottawa) provided the carbon isotope

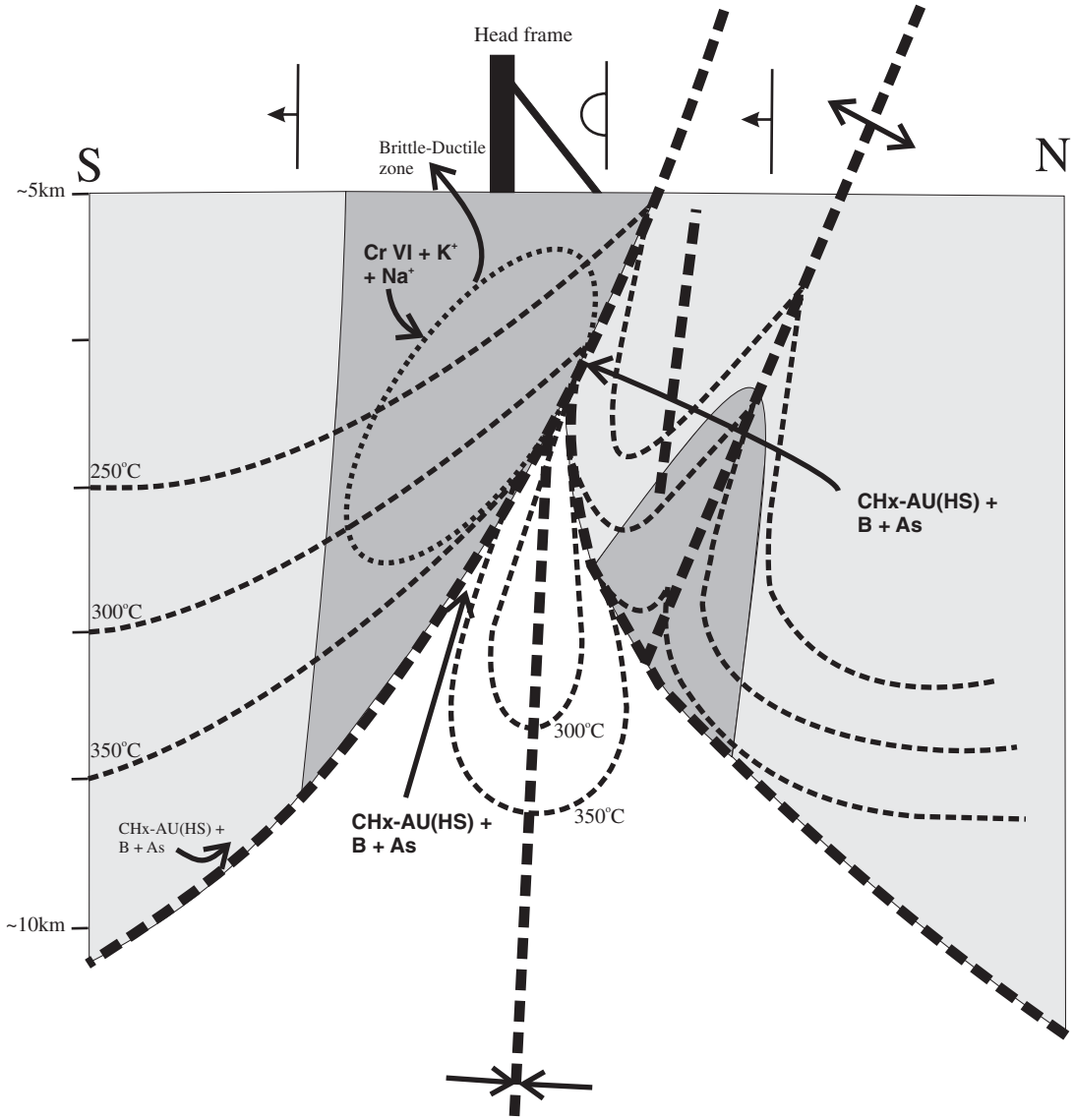

FIG. 16. A schematic illustration of the structure in the Hoyle Pond area (not to scale), during D_3 and D_4 indicating possible geothermal gradients and flow lines for hydrothermal fluids containing Au, B, and As, as well as sites of deposition of metals as well as Cr, K, and Na in the brittle-ductile transition zone.

analysis. Benoit-Michel Saumur provided able field assistance during the summer of 2004.

The research was financed by a cooperative research development grant from the Porcupine Joint Venture and the Natural Science and Engineering Research Council to ADF for which we are grateful.

REFERENCES

Anderson, J.R., 1975, Structure of metallic catalyst: New York, Academic Press, 469 p.

Arndt, N.D., 1975, Ultramafic rocks of Munro Township and their volcanic setting: Unpublished Ph.D. thesis, Toronto, Ontario, University of Toronto, 192 p.

Ayer, J.A., Thurston, P.C., Bateman, R., Dubé, B., Gibson, H.L., Hamilton, M.A., Hathway, B., Hocker, S.M., Houlé, M.G., Hudak, G., Ispolatov, V.O., Lafrance, B., Lesher, C.M., MacDonald, P.J., Péloquin, A.S., Piercey, S.J., Reed, L.E., and Thompson, P.H., 2005, Overview of results from the Greenstone Architecture Project: Discover Abitibi Initiative: Ontario Geological Survey Open File Report 6154, 175 p.

Bateman, R., Ayer, J.A., Barr, E., Dubé, B., and Hamilton, M.A., 2005, The Timmins-Porcupine gold camp, northern Ontario: the anatomy of an Archean greenstone belt and its gold mineralization: Discover Abitibi Initiative: Ontario Geological Survey Open File Report 6158, 90 p.

Bleeker, W., 1999, Structure, stratigraphy and primary setting of the Kidd Creek volcanogenic massive sulfide deposit: A semiquantitative reconstruction: Economic Geology Monograph 10, p. 71–122.

Bohlke, J.K., 1989, Comparison of metasomatic reactions between a common CO_2-rich vein fluid and diverse wall rocks: Intensive variables, mass transfers, and Au mineralization at Alleghany, California: Economic Geology, v. 84, p. 291–327.

Born, P., 1995, A sedimentary basin analysis of the Abitibi greenstone belt in the Timmins area, northern Ontario, Canada: Unpublished Ph.D. thesis, Ottawa, Carleton University, 489 p.

Brisbin, D.I., 1997, The geological setting of gold deposits in the Porcupine gold camp, Timmins, Ontario: Unpublished Ph.D. thesis, Kingston, ON, Queen's University, 523 p.

Deer, W.A., Howie, R.A., and Zussman, J., 1992, An introduciton to the rock-forming minerals, 2nd ed.: New York, Longman Scientific and Technical, 696 p.

Dinel, E., 2001, Structural investigation of the Echo Bay and international properties, Timmins, Ontario: Unpublished B.Sc. thesis, Ottawa, Ontario, University of Ottawa, 20 p.

——2007, A litho-geochemical, alteration and structural investigation of the Hoyle Pond gold mine, Timmins, Ontario: Controls on mineralization within meta-volcanic rocks: Unpublished Ph.D. thesis, Ottawa, Ontario, University of Ottawa, 248 p.

Dinel, E., Saumur, B.M., and Fowler, A.D., 2008, Spherulitic aphyric pillow lobe metatholeiitic dacite lava of the Timmins area, Ontario, Canada: A new Archean facies formed from superheated melts: Economic Geology, v. 103, p. 1365–1378.

Downes, M.J., Hodges, D.J., and Derweduwen, J., 1984, A free carbon- and carbonate-bearing alteration zone associated with the Hoyle Pond gold occurrence, Ontario, Canada, *in* Foster, R.P., ed., Gold '82: The geology, geochemistry and genesis of gold deposits: Rotterdam, A. A. Balkema, p. 435–448.

Dunbar, R.D., 1948, Structural relations of the Porcupine ore deposits, *in* Wilson, M.E., ed., Structural geology of Canadian ore deposits: Montreal, Quebec, Canadian Institute of Mining and Metallurgy Symposium, Jubilee Volume, p. 442–456.

Farmer, B.C., and Morrison, R.I., 1960, Chemical and infrared on phramites peat and its humic acid: Science Proceeding Royal Dublin Society, Series A1, p. 85–104.

Faure, G., 1998, Principles and applications of geochemistry, 2nd ed.: Prentice Hall, 600 p.

Ferguson, S.A., Buffman, B.S.W., Carter, O.F., Griffis, A.T., Holmes, T.C., Hurst, M.E., Jones, W.A., Lane, H.C., and Longley, C.S., 1968, Geology of ore deposits of Tisdale Township, District of Cochrane. Timmins: Ontario Department of Mines Geological Report 58, 117 p.

Fowler, A.D., and Doig, R., 1983, The significance of Europium anomalies in the REE spectra of granites and pegmatites, Mont Laurier, Québec: Geochimica et Cosmochimica Acta, v. 47, p. 1131–1137.

Grant, G.A., 1986, The isocon diagram—a simple solution to Gresen's equations for metasomatic alteration: Economic Geology, v. 82, pp. 1976–1982.

Henry, S., 2000, Influence de la vapeur d'eau sur l'oxydation à haute température du chrome et de quelques aciers inoxydables férritiques stabilisés: Unpublished Ph.D. thesis, Grenoble, France, Institut national polytechnique de Grenoble, 190 p.

Hodges, D.J., 1982, Alteration associated with gold mineralization near the Owl Creek deposit: Unpublished B.Sc. thesis, Waterloo, ON, University of Waterloo, 39 p.

Jensen, L.S., 1976, A new cation plot for classifying subalkalic volcanic rocks: Ontario Department of Mines Miscellaneous Paper 66, 22 p.

Jones, W.A., 1948, Hollinger mine: Montreal, Canadian Institute of Mining and Metallurgy Special Volume 1, p. 464–481.

Kim, C., Zhou, Q., and Deng, B., 2001, Chromium(VI) reduction by hydrogen sulfide in aqueous media: Stoichiometry and kinetics: Environmental Science and Technology, v. 35, p. 2219–2225.

Kerrich R., Wyman, D., and Hollings, P., 1999, Trace elements systematics of Mg-, to Fe-tholeiitic basal suites of the Superior province: Implications for Archean mantle reservoirs and greenstone belt genesis: Lithos, v. 46, p. 163–187.

Kretz, R., 1985, Calculation and illustration of uncertainty in geochemical analysis: Journal of Geological Education, v. 33, p. 40–44.

McCuaig, T.C, and Kerrich, R., 1998, P-T-t-deformation-fluid characteristics of lode gold deposits: Evidence from alteration systematics: Ore Geology Reviews, v. 12, p. 381–453.

Melnik-Proud, N., 1992, The geology and ore controls in and around the McIntyre mine at Timmins, Ontario, Canada: Unpublished Ph.D. thesis, Kingston, ON, Queen's University, 353 p.

Michard, A., and Albarède, F., 1986, The REE content of some hydrothermal fluids: Chemical Geology, v. 55, p 51–65.

Moritz, R.P., and Crocket, J.H., 1991, Hydrothermal wall-rock alteration and formation of the gold-bearing quartz-fuchsite vein at the Dome mine, Timmins area, Ontario, Canada: Economic Geology, v. 86, p. 620–643.

Olivo, G.M., and Williams-Jones, A.E., 2002, Genesis of the auriferous C quartz-tourmaline vein of the Siscoe mine, Val d'Or district, Abitibi subprovince, Canada: Structural, mineralogical, and fluid inclusion constraints: Economic Geology, v. 97, p. 929–947.

Pyke, D.R., 1982, Geology of the Timmins area, District of Cochrane: Ontario Geological Survey Report 219, 141 p.

Robert, F., 2001, Syenite-associated disseminated gold deposits in the Abitibi greenstone belt, Canada: Mineralium Deposita, v. 36, p. 503–516.

Ropchan J.R., Fowler A.D., Benn K., Ayer J., Berger B., Dahn, R., Labine, R., and Amelin, Y., 2002, Host rock and structural controls on the nature and timing of gold mineralization at the Holloway mine, Abitibi subprovince, Ontario: Economic Geology, v. 97, p. 291–309.

Rye, K.A., 1987, Geology and geochemistry of the Hoyle Pond gold deposit, Timmins, Ontario: Unpublished M.Sc. thesis, London, University of Western Ontario, 220 p.

Sapek, B., Sapek, A., and Okruzko, H., 1980, Optical properties of alkaline soil extracts as a test characterizing humic substances from peat soils: International Peat Society Meeting, 6th, Duluth, Minnesota, August 1980, Proceedings, 735 p.

Sass, B.M., and Rai, D., 1987, Solubility of amorphous chromium(III)-iron(III) hydroxide solid solutions: Inorganic Chemistry, v. 26, p. 2228–2232.

Seward, T.M., 1973, Thio complexes of gold and the transport of gold in hydrothermal ore solutions: Geochimica et Cosmochimica Acta, v. 37, p.379–399.

Shelton, K.L., McMenamy, T.A., Van Hees, E.H.P., and Falck, H., 2004, Deciphering the complex fluid history of a greenstone-hosted gold deposit: Fluid inclusion and stable isotope studies of the Giant Mine, Yellowknife, Northwest Territories, Canada, v. 99, p 1643–1663.

Sun, S.S., and McDonough, W.F., 1989, Chemical and isotopic systematics and oceanic basalts: Implications for mantle composition and processes, *in* Saunders, A.D., and Norry, M.J., eds., Magmatism in the ocean basins: London, Geological Society of London, p. 315–345.

Szulczewski, M.D., Helmke, P.A., and Bleam, W.F., 2001, XANES spectroscopy studies of Cr (VI) reduction by thiol in organosulphur compounds and humic substances: Environmental Science Technology, v. 35, p. 1134–1141.

Thompson, P.H., 2005, A new metamorphic framework for gold exploration in the Timmins-Kirkland Lake area, western Abitibi greenstone

belt: Discover Abitibi Initiative: Ontario Geological Survey Open File Report 6162, 104 p.

Thornton, E.C., and Amonette, J.E., 1999, Hydrogen sulfide gas treatment of Cr.(VI)-contaminated sediment samples from a plating-waste disposal site—implications for in-situ remediation: Environmental Science Technology, v. 33, p. 4096–4101.

Vaillancourt, C., Pickett, C.L., and Dinel, E., 2001, Precambrian geology; Timmins, West-Bristol, and Ogden Townships: Ontario Geological Survey Report P3436.

Van Hees, E.H.P., Shelton, K.L., McMenamy, T.A., Ross, L.M., Cousens, B.L., Falck, H., Robb, M.E., and Canam, T.W., 1999; Metasedimentary influence on metavolcanic-rock-hosted greenstone gold deposits: Geochemistry of the Giant mine, Yellowknife, Northwest Territories, Canada: Geology, v. 27, p. 71–74.

Whipple, E.R., 1974, A study of Wilson's determination of ferrous iron silicates: Chemical Geology, v. 14, p. 119–134.

Wilson, A.D., 1960, The micro-determination of ferrous iron in minerals by a volumetric and calorimetric method: Analyst, v. 85, p. 823–827.

Wyman, D.A., 2003, Upper mantle processes beneath the 2.7 Ga Abitibi belt, Canada: A trace element perspective: Precambrian Research, v. 127, p. 143–165.

Zouboulis, A.I., Kydros, K.A., and Matis, K.A., 1995, Removal of hexavalent chromium anions from solutions by pyrite fines: Water Resource, v. 29, p. 1755–1760.